Resource

Developmental Cell

Studying the Fate of Tumor Extracellular Vesicles at High Spatiotemporal Resolution Using the Zebrafish Embryo

Graphical Abstract

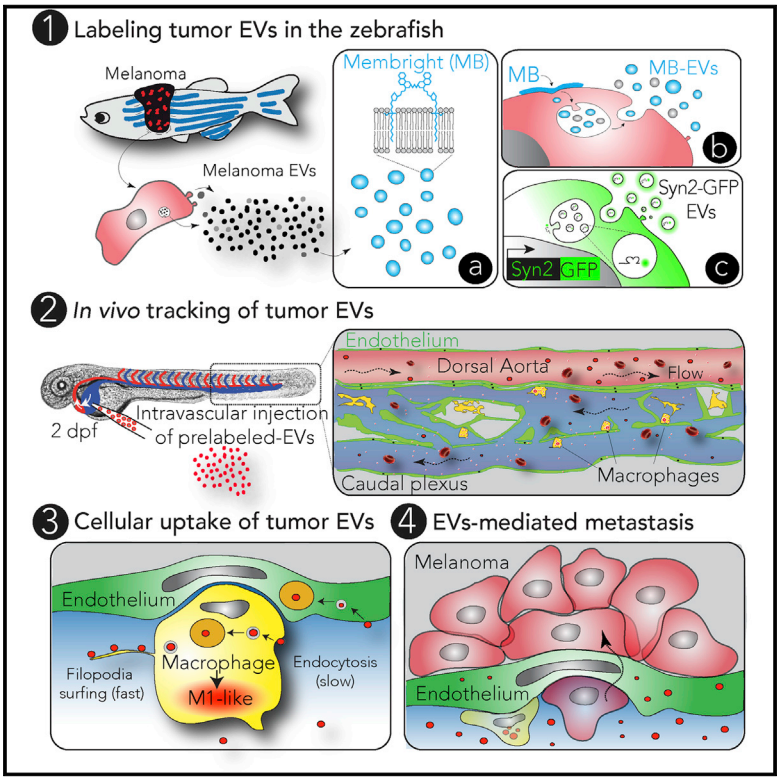

Highlights

- MemBright allows for bright and specific staining of EVs
- The zebrafish embryo allows tracking of tumor EVs at high spatiotemporal resolution
- Circulating tumor EVs are mostly taken up by endothelial cells and patrolling macrophages
- Zebrafish melanoma EVs favor metastatic outgrowth in zebrafish embryos

Authors

Vincent Hyenne, Shima Ghoroghi, Mayeul Collot, ..., Christine Carapito, Andrey S. Klymchenko, Jacky G. Goetz

Correspondence

hyenne@unistra.fr (V.H.), jacky.goetz@inserm.fr (J.G.G.)

In Brief

Tumor extracellular vesicles (EVs) promote tumor progression. However, their behavior in body fluids remains mysterious. Hyenne et al. show that the zebrafish embryo can be used to track and assess the function of circulating tumor EVs *in vivo* and provide a high-resolution description of their dissemination and uptake.

Hyenne et al., 2019, Developmental Cell *48*, 554–572
February 25, 2019
https://doi.org/10.1016/j.devcel.2019.01.014

CellPress

CellPress

Developmental Cell
Resource

Studying the Fate of Tumor Extracellular Vesicles at High Spatiotemporal Resolution Using the Zebrafish Embryo

Vincent Hyenne,[1,2,3,4,12,*] Shima Ghoroghi,[1,2,3] Mayeul Collot,[5] Joanna Bons,[6] Gautier Follain,[1,2,3] Sébastien Harlepp,[1,2,3] Benjamin Mary,[1,2,3] Jack Bauer,[1,2,3] Luc Mercier,[1,2,3] Ignacio Busnelli,[1,2,3] Olivier Lefebvre,[1,2,3] Nina Fekonja,[1,2,3] Maria J. Garcia-Leon,[1,2,3] Pedro Machado,[7] François Delalande,[6] Ana Amor López,[8] Susana Garcia Silva,[8] Frederik J. Verweij,[9,10] Guillaume van Niel,[9,10] Farida Djouad,[11] Héctor Peinado,[8] Christine Carapito,[6] Andrey S. Klymchenko,[5] and Jacky G. Goetz[1,2,3,*]

[1]INSERM UMR_S1109, Strasbourg 67200, France
[2]Université de Strasbourg, Strasbourg 67200, France
[3]Fédération de Médecine Translationnelle de Strasbourg, Strasbourg 67200, France
[4]CNRS SNC5055, Strasbourg 67200, France
[5]Laboratoire de Biophotonique et Pharmacologie, UMR CNRS 7213, Université de Strasbourg, Illkirch 67000, France
[6]CNRS, Laboratoire de Spectrométrie de Masse Bio-Organique (LSMBO), IPHC, UMR 7178, Université de Strasbourg, Strasbourg 67087, France
[7]Electron Microscopy Core Facility, European Molecular Biology Laboratory, Heidelberg 69117, Germany
[8]Microenvironment and metastasis group. Department of Molecular Oncology, Spanish National Cancer Research Center (CNIO), Madrid, Spain
[9]Institut Curie, PSL Research University, CNRS UMR144, Paris 75005, France
[10]Center for Psychiatry and Neuroscience, Hôpital Saint-Anne, Université Descartes, INSERM U894, Paris 75014, France
[11]IRMB, Université de Montpellier, INSERM, Montpellier, France
[12]Lead Contact
*Correspondence: hyenne@unistra.fr (V.H.), jacky.goetz@inserm.fr (J.G.G.)
https://doi.org/10.1016/j.devcel.2019.01.014

SUMMARY

Tumor extracellular vesicles (EVs) mediate the communication between tumor and stromal cells mostly to the benefit of tumor progression. Notably, tumor EVs travel in the bloodstream, reach distant organs, and locally modify the microenvironment. However, visualizing these events *in vivo* still faces major hurdles. Here, we describe an approach for tracking circulating tumor EVs in a living organism: we combine chemical and genetically encoded probes with the zebrafish embryo as an animal model. We provide a first description of tumor EVs' hemodynamic behavior and document their intravascular arrest. We show that circulating tumor EVs are rapidly taken up by endothelial cells and blood patrolling macrophages and subsequently stored in degradative compartments. Finally, we demonstrate that tumor EVs activate macrophages and promote metastatic outgrowth. Overall, our study proves the usefulness and prospects of zebrafish embryo to track tumor EVs and dissect their role in metastatic niches formation *in vivo*.

INTRODUCTION

Over the past two decades, extracellular vesicles (EVs) have emerged as novel mediators of cell-cell communication due to their capacity to carry functional molecules coupled with their ability to travel in biological fluids (Raposo and Stoorvogel, 2013). EVs are heterogeneous in content and origin, as they can either arise from plasma membrane budding (then called microvesicles) or originate from a late endosomal compartment, the multi-vesicular body (MVB) (i.e., exosomes) (van Niel et al., 2018). EVs are known to be important in tumor progression and metastasis, where the complex tumor microenvironment requires a permanent cross-communication between cells (Hyenne et al., 2017). EVs secreted by tumor cells are enriched in pro-tumoral and pro-metastatic factors (proteins, mRNAs, miRNAs, and other non-coding RNAs) and can modify the phenotype of both tumor and stromal cells, mostly to the benefit of tumor growth and metastasis formation (Hyenne et al., 2017). For instance, tumor EVs were shown to transfer oncogenic traits from more aggressive to less aggressive tumor cells (Al-Nedawi et al., 2008). Importantly, tumor EVs can differentiate macrophages or fibroblasts into tumor-associated macrophages or fibroblasts, thereby promoting tumor growth and invasion (Chow et al., 2014; Gu et al., 2012; Paggetti et al., 2015). This pro-metastatic EV-mediated communication can occur within the primary tumor or at distance in physically far-off organs (Peinado et al., 2017). Remarkably, repeated injection of EVs isolated from metastatic cells into the mouse blood circulation induces the formation of a pre-metastatic niche, even in the absence of tumor cells (Costa-Silva et al., 2015; Grange et al., 2011; Hoshino et al., 2015; Liu et al., 2016; Peinado et al., 2012). The ability of circulating tumor EVs to alter the microenvironment of a given organ is particularly relevant with regard to (1) the increased amounts of tumor EVs present in the blood circulation of patients with cancer (Baran et al., 2010; Galindo-Hernandez et al., 2013;

Logozzi et al., 2009), and (2) the fact that elevated levels of EV proteins have been associated with poor prognosis in metastatic melanoma patients (Peinado et al., 2012). Therefore, it is crucial to precisely understand the mechanisms governing tumor EV dispersion and uptake in the blood circulation.

However, local or distant dissemination of tumor EVs has only been sparsely characterized in living organisms (Hoshino et al., 2015; Lai et al., 2015; Pucci et al., 2016). In particular, how EVs circulate in the blood flow and how specifically they are internalized by stromal cells during the priming of pre-metastatic niches remain poorly understood. EVs are nanoscale objects and are thus difficult to track *in vivo*. Moreover, mouse models are not fully suited for real time and *in vivo* EV tracking. In mice, EVs can either be followed after bulk injections (Lai et al., 2014; Takahashi et al., 2013) or with increased resolution through intravital imaging procedures (Lai et al., 2015; Van Der Vos et al., 2016; Zomer et al., 2015). However, such approaches have not yet been able to describe the behavior of tumor EVs in the blood circulation. An ideal animal model suited to accurately dissect the behavior of tumor EVs *in vivo* would allow their tracking in the circulation and their uptake and, at the same time, be amenable for modeling tumor and metastasis progression.

Interestingly, the zebrafish embryo largely complies with all these needs. Indeed, zebrafish has recently emerged as a potent model in cancer biology (White et al., 2013). The molecular pathways driving cancer progression and the anatomo-pathological features of tumorigenesis are essentially conserved between human and fish. In addition, the zebrafish embryo is transparent, possesses a stereotyped vasculature, a maturating immune system and is therefore perfectly suited for intravital imaging with high spatial and temporal resolution. For these reasons, the zebrafish embryo appears as an adequate model to study tumor EVs *in vitro*.

Here, we show that zebrafish melanoma EVs are similar to human melanoma EVs and demonstrate how their fate can be tracked in the zebrafish embryo. For efficient staining of EVs, we used MemBright, a recently developed cyanine-based membrane probe with improved brightness and specificity (Collot et al., 2019). Using this tool, and EVs from genetically engineered cells in parallel, we provide the first description of EVs' dynamics in the blood circulation. We subsequently examined the transit routes and arrest sites of tumor EVs and identified endothelial cells and patrolling macrophages as major EVs-recipient cells. Importantly, these cells have also been identified in a parallel study describing endogenous EVs dispersion in the zebrafish embryo (Verweij et al., 2019). We further show that these cell types have increased uptake efficiency toward tumor EVs, and found that patrolling macrophages internalize tumor EVs through at least two distinct endocytic mechanisms, before storing them in acidic compartments. Using correlated light and electron microscopy (CLEM), we precisely identified the cells uptaking EVs and finely described their morphology as well as the storage or degradative compartments at the electron microscopy level. In addition, we demonstrate that it is possible to track naturally released EVs *in vivo* in the zebrafish embryo using either pre-labeling with MemBright or genetically engineered cells. Finally, we show that melanoma EVs activate macrophages and promote metastatic outgrowth in zebrafish.

RESULTS

Zebrafish Melanoma EVs Are Similar to Human and Mouse Melanoma EVs

To study tumor EVs in zebrafish, we first characterized EVs released by a melanoma cell line (Zmel1) derived from a transgenic mitfa-BRAF(V600E);p53(−/−) zebrafish line (Heilmann et al., 2015) (Figure 1A). EVs were isolated from a cell culture supernatant following an established protocol of differential centrifugation (Théry et al., 2006), and EVs present in the 100.000 g pellet were characterized by nanoparticle tracking analysis (NTA) and electron microscopy. We found that Zmel1 EVs have an average diameter of 150 nm in solution and 90 nm after chemical fixation (Figures 1B and 1C). Subsequently, we characterized the protein content of these EVs by mass spectrometry and identified 794 proteins present in Zmel1 EVs (Table S1A). This list includes several proteins typically found in extracellular vesicles, such as ALIX, CD81, Flotillin 1, TSG101, CD9, RalA, Hsc70, HSP90, syntenin 2, integrins α5 and β1, and others (of note, CD63 was absent from Zmel1 EVs) (Figure 1D; Table S1A). We then wondered whether the content of zebrafish melanoma EVs was comparable to the ones of human or mouse melanoma EVs. We compared proteins present in Zmel1 EVs with proteins identified in the EVs isolated from six human (451-LU, SK-Mel28, SK-Mel147, SK-Mel103, WM35, and WM164) (Tables S1B–S1G) and three mouse (B16-F0, B16-F1, and B16-F10) (Tables S1H–S1J) melanoma cell lines. Protein content comparison revealed that 65% and 40% of Zmel1 proteins were also identified in human or mouse melanoma EVs, respectively (Figure 1E). Zmel1 EVs are closer to human melanoma EVs than to mouse melanoma EVs. We identified a core list of 82 proteins found in melanoma EVs from either zebrafish, mice, or human (Table S1K). Altogether, these data demonstrate that Zmel1 EVs derived from an established zebrafish melanoma cell line are highly similar to mammalian melanoma EVs and therefore constitute a good model to study human melanoma EVs.

In addition, we compared proteins present in Zmel1 EVs with proteins present in two other types of zebrafish EVs identified in a parallel study (Verweij et al., 2019). First, 17% of Zmel1 EVs proteins are also present in EVs from AB9 fibroblastic cell line (Table S1L). Then, we compared Zmel1 EVs with CD63-positive EVs secreted by a zebrafish embryonic epithelium, the yolk syncytial layer (YSL), and isolated from zebrafish embryos (Verweij et al., 2019). Interestingly, we found a relatively low similarity between these two types of zebrafish EVs (1–2% of Zmel1 EV proteins are present in YSL CD63+EVs; 10% of YSL CD63+EV proteins are present in Zmel1 EVs) (Table S1M). This difference illustrates the cell-type specificity of EV cargo enrichment. However, the mechanism of biogenesis of these two EV types could be partially similar, as 5 of the 12 proteins common to Zmel1 EVs and YSL EVs have been shown to affect, positively or negatively, exosome secretion in mammalian cells: TSG101, ALIX, Syntenin 2, Flotillin 1, and Rab2 (Baietti et al., 2012; Colombo et al., 2013; Okabayashi and Kimura, 2010; Ostrowski et al., 2010).

The MemBright Dye Specifically and Brightly Labels Tumor EVs

In order to fluorescently label Zmel1 EVs and follow them *in vivo*, we used new membrane probes, MemBright (Collot et al., 2019).

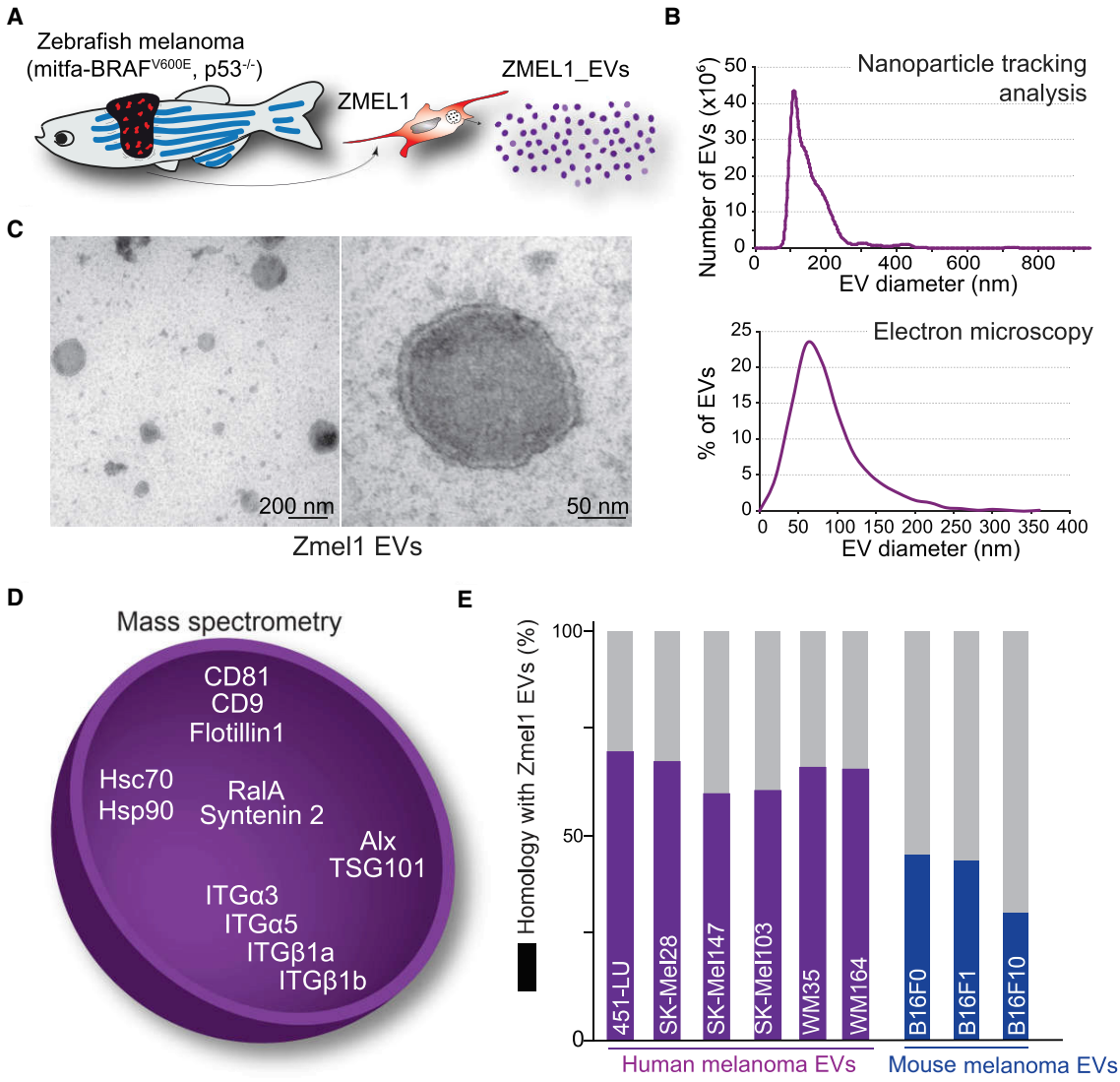

Figure 1. EVs Secreted by Zmel1 Zebrafish Melanoma Cells Are Similar to Mouse and Human Melanoma EVs

(A) Zebrafish melanoma EVs were isolated from Zmel1 cells by differential centrifugation (Heilmann et al., 2015).

(B) Histogram of a nanoparticle tracking analysis of Zmel1 EVs showing the number of EVs (y axis) versus their diameter (nm, x axis).

(C) Electron microscopy images of Zmel1 EVs and a histogram showing the percentage of total EVs (y axis) versus their diameter (nm, x axis).

(D) Illustration of some of the classical EV proteins present among the 794 proteins identified in ZMel1 EVs by mass spectrometry (see Table S1).

(E) Histogram showing the percentage of Zmel1 EVs proteins common with EV proteins from various human or mouse cell lines (using human orthologs).

They differ significantly from existing commercial dyes because they bear two amphiphilic groups composed of zwitterions and alkyl chains, which insert the dye into the membrane bilayer (Figure 2A). Moreover, MemBright is available in several colors, which therefore enables multi-color approach in EV imaging (Figures S2G–S2I). To assess the value of MemBright in EV labeling, we first globally compared the MemBright-labeled EVs to identical EVs labeled with PKH-26, a commercially available and widely used dye for EV labeling (Hoshino et al., 2015; Imai et al., 2015). Zmel1 EVs were incubated with MemBright-Cy3 (at 0.2 μM) or with PKH-26 (at 2 μM, according to manufacturer's instructions), washed and isolated by ultracentrifugation. Using fluorescence spectroscopy, we observed that PKH-labeled EVs display a broad absorption spectrum, with a blue shifted peak typically indicating the presence of H-aggregation (Figure 2B) (Würthner et al., 2011). By contrast, MemBright-labeled EVs show an absorption spectrum identical to the solubilized form of the probe (Figures 2B and S1A), revealing that the MemBright is efficiently embedded in EV membranes. MemBright-labeled EVs are as bright as PKH-labeled EVs even though the MemBright was 10-fold less concentrated than PKH (Figures 2B, 2C, and S1D). When both dyes were used at similar dilutions (0.2 μM), the MemBright labeled EVs were much brighter than the PKH ones (Figure S1E). Indeed, MemBright displays >20-fold higher quantum yield than the PKH: 0.42 versus 0.02 (Table S2). Since MemBright-Cy3 and

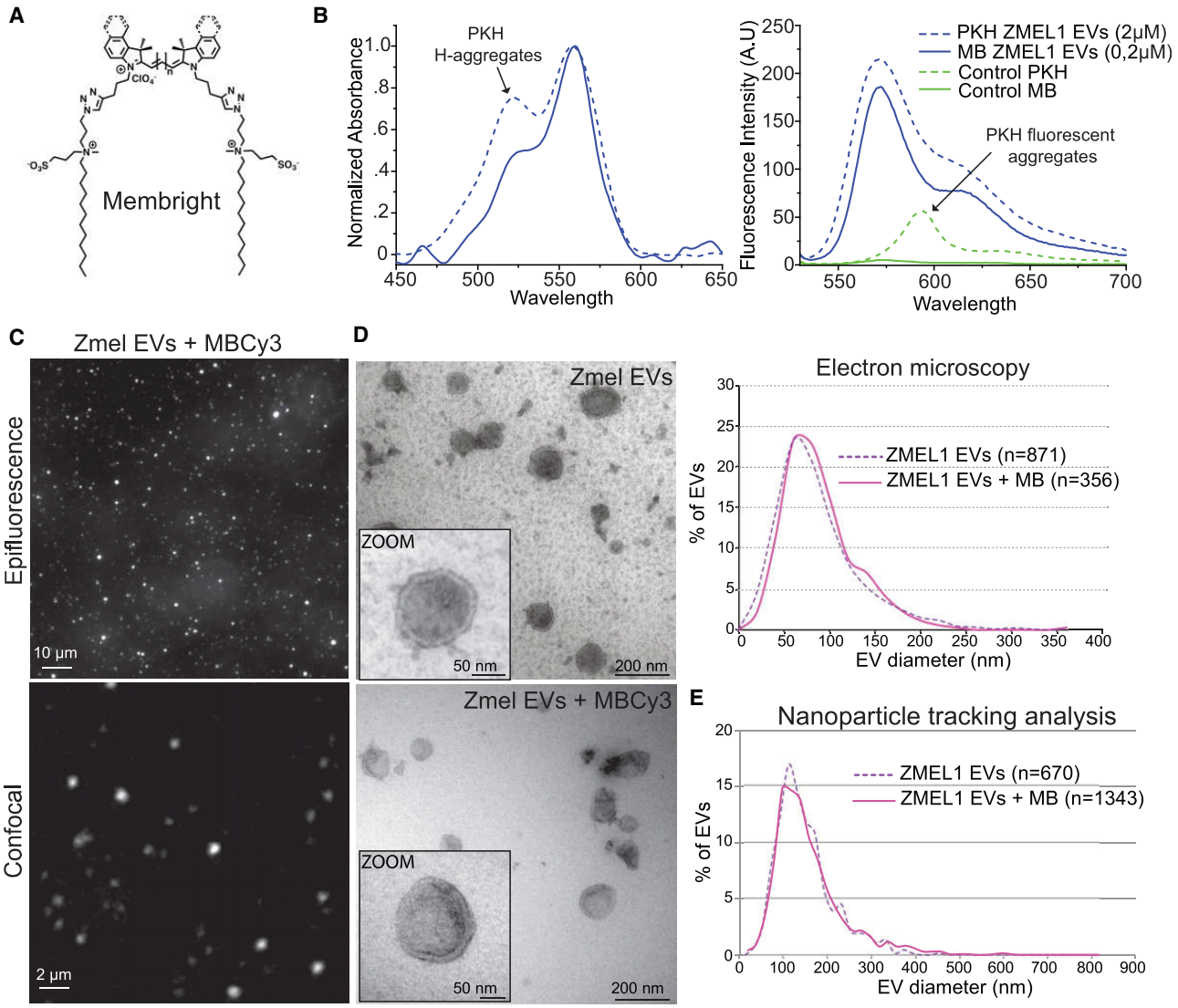

Figure 2. EVs Can Be Brightly and Specifically Labeled with MemBright

(A) Molecular structure of the membrane binding probe MemBright.

(B) Histograms showing a spectroscopy analysis of MemBright (MB) and PKH labeled Zmel1 EVs describing the absorbance (left histogram, y axis) and the fluorescence intensity (right histogram, y axis) versus the wavelength (nm, x axis). Arrows indicate the presence of PKH aggregates in labeled EVs (left) as well as in control PKH alone (right).

(C) Zmel1 EVs labeled with MemBright Cy3 (MBCy3) observed by Epifluorescence (upper) and confocal (lower).

(D) Electron microscopy of non-labeled (upper) and labeled (lower) Zmel1 EVs and histogram showing the percentage of labeled and non-labeled Zmel1 EVs (y axis) versus their diameter (x axis, nm) by electron microscopy (right graph).

(E) Nanoparticle tracking analysis of MemBright-labeled and non-labeled Zmel1 EVs showing the number of EVs (y axis) versus their diameter (nm, x axis).

PKH26 contain the same Cy3-based fluorophore, such remarkable difference in the quantum yield suggests inefficient partitioning of PKH into EV membranes. This poor partitioning probably arises from the aggregation of PKH in aqueous media, in line with characteristic short-wavelength shoulder in the absorption spectrum in the samples of EVs (Figure S1B). This is not the case for MemBright. Interestingly, a similar spectroscopic experiment conducted without EVs reveals the presence of a red-shifted fluorescence peak with PKH alone but not with MemBright alone (Figure S1C). These fluorescent PKH aggregates have an average diameter of 80 nm (± 10 nm), as analyzed by fluorescence correlation spectroscopy (FCS), which is in the range of EVs and therefore could lead to artifacts. To complement these studies, we analyzed MemBright-labeled EVs by electron microscopy and NTA and found that neither their morphology nor their size was affected, when compared to non-labeled EVs (Figure 2D). Importantly, no larger size aggregates were detected in MemBright-labeled EVs (Figure 2E). Finally, we demonstrated the versatility of MemBright by labeling EVs isolated from 4T1 mouse mammary carcinoma cells. Spectroscopy (Figure S1B; Table S2) and electron microscopy analysis (data not shown) confirmed the advantages of the

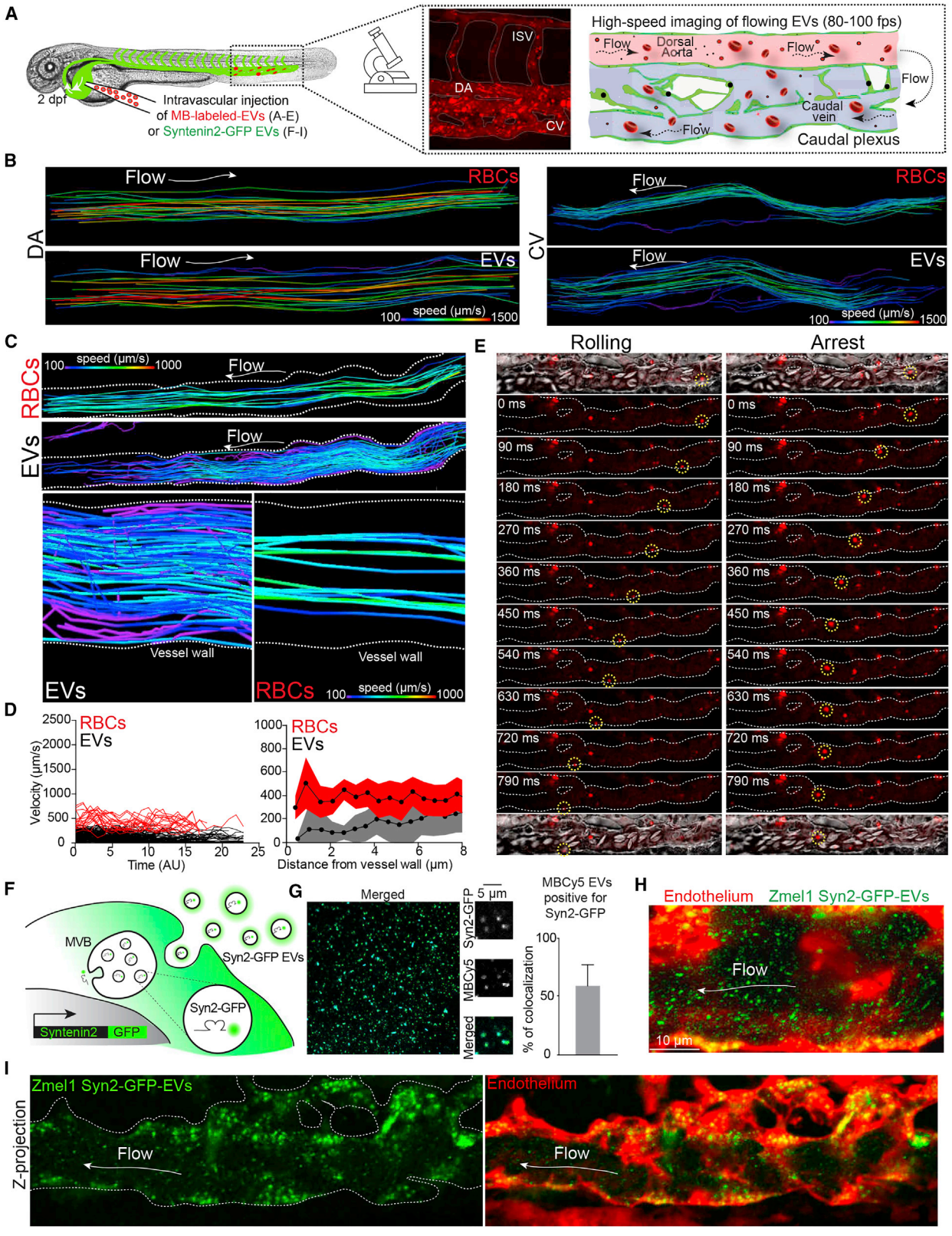

(legend on next page)

MemBright probes. Furthermore, separation of MemBright-labeled 4T1 EVs by density gradient revealed that the majority of the fluorescent MemBright is present in the fractions where most EVs are found, as confirmed by the presence of ALIX and TSG101 (Figure S1F). Altogether, these experiments prove that labeling EVs with MemBright does not lead to soluble fluorescent aggregates that can be confounded with labeled EVs. In addition, given its high quantum yield, MemBright can be used at a relatively low concentration to efficiently label isolated EVs.

Tumor EVs Can Be Individually Tracked in the Living Zebrafish Embryo

We next investigated whether MemBright labeling could be used for tracking tumor EVs *in vivo*. We injected zebrafish embryos at 2 days post-fertilization with MemBright-labeled EVs in the blood circulation. Fluorescent EVs were observed essentially in the tail region of the embryo, which is composed of the dorsal aorta and the venous caudal plexus (Figure 3A). Minutes following injection, we observed several fluorescent EVs that were either still flowing or that were already arrested along the endothelium (Figure 3A; Video S1A). We first assessed the apparent size of EVs by comparing them to 100 nm fluorescent polystyrene beads. *In vitro* and upon injection in the circulation of zebrafish embryos, we found that MemBright-labeled EVs and 100 nm fluorescent beads display similar apparent sizes, which correspond to the resolution limits of confocal microscopy (Figures S2A–S2D). Furthermore, MemBright-labeled EVs do not adhere to red blood cells (RBCs), and no leakage of MemBright from EVs to RBCs could be observed *in vitro* or *in vivo* (Figures S2E and S2F). These observations suggest that MemBright in combination with our microscopy set-up allow imaging of fluorescent objects of the size of an individual EV. At this stage, however, we cannot assess whether bigger spots result from bigger EVs or clusters of small EVs. In addition, MemBright can be used to co-inject different types of EVs labeled with different colors (Cy3, Cy5) and specifically track their fate. As a proof of concept, we co-injected Zmel1 tumor EVs (labeled with MemBright-Cy5) with 4T1 mouse tumor EVs (labeled with MemBright-Cy3) in zebrafish embryos and observed both specific localizations for each EVs population as well as a common uptake in isolated cells (Figures S2H and S2I). This suggests that MemBright could be used to follow specific internalization routes of distinct types of EVs that might be on the basis of their function and message delivery.

We then aimed to describe the over-looked behavior of tumor EVs in the blood circulation. To do that, we performed high-speed confocal acquisitions of flowing tumor EVs (and of co-flowing RBCs) in different regions of the vasculature of living zebrafish embryos (Figure 3A; Videos S1B and S1C). When tracking both tumor EVs and RBCs, we first found that EVs have a higher velocity in the aorta than in the caudal veins, in accordance with the hydrodynamic profiles previously described in this region of the zebrafish embryo vasculature (Figure 3B) (Follain et al., 2018a). Second, when analyzing co-motion of tumor EVs and RBCs in a single vessel, we noticed that EVs have a reduced velocity compared to RBCs. These observations are not restricted to Zmel1 EVs since 4T1 EVs display a higher velocity in the dorsal aorta than in the caudal veins but a slower velocity than RBCs (Figures 3C and 3D). Interestingly, we observed that the hemodynamic behavior of tumor EVs differs in regions close to the vessel wall, from which RBCs are mostly excluded. Indeed, when we plotted the velocity of tumor EVs as a function of their position with regards to vessel walls, we observed that tumor EVs explore the vicinity of vessel walls with a reduced velocity (Figures 3C and 3D). Thus, it seems that tumor EVs follow a Poiseuille flow, which predicts that objects displaced by a laminar flow would have a reduced velocity because of frictional forces, along the border of the vessel wall. Such a behavior, in addition to their potential adhesive capacity, could thus favor the arrest of tumor EVs. Indeed, individual inspection of EVs in close proximity to the vessel wall reveals that they are either flowing, rolling on the surface of the endothelium, or arresting (Figure 3E). We observed arrest of EVs following a rolling behavior, suggesting that it could be driven by progressive activation of adhesion molecules, as well as the sharp arrest of flowing EVs, without a rolling phase (Video S2). A very similar behavior was observed for endogenous EVs (Verweij et al., 2019). Altogether, we provide the first accurate description of circulating tumor EVs in the vasculature.

In addition, we used a complementary genetic approach. We expressed Syntenin2 (a major cargo detected in Zmel1 EVs by mass spectrometry, Figure 1D) fused to GFP in Zmel1 cells and showed that these cells secrete GFP-positive EVs (Figures 3F and 3G). Upon intravascular injection in zebrafish embryos, the Syntenin2-GFP EVs can be tracked in the circulation similar to MemBright-labeled EVs (Figures 3H and 3I). Altogether, we document that both genetically and chemically labeled tumor

Figure 3. Hemodynamic Characterization of Individual EVs Tracked in the Circulation of Zebrafish Embryo

(A) Experimental setup used to track circulating EVs: two days post-fertilization zebrafish embryos are injected in the duct of Cuvier with fluorescent EVs (left) and observed in the caudal plexus with high-speed confocal microscopy. Middle: *Z* projection of MemBright-Cy3 Zmel1 EVs in the caudal plexus right after injection. Right: schematic representation of the caudal plexus showing the direction of the blood flow in the dorsal aorta (pink) and the venous plexus (blue).

(B) Individual tracks of red blood cells (RBC) or Zmel1 EVs in the dorsal aorta (DA, left) and in the caudal vein (CV, right).

(C) Upper: Individual tracks of red blood cells (RBC) or 4T1 EVs in the CV. Lower: Zoom on individual tracks of red blood cells (RBC, right) or 4T1 EVs (left) in the CV in proximity of the vessel wall (white lines). (B) and (C): Color coding represents velocities.

(D) Left: histogram showing the velocity (y axis, μm/s) versus the time (x axis, AU) of RBCs (red) and EVs (black) in the CV. Right: histogram showing the velocity (y axis, μm/s) versus the distance to the vessel wall (x axis, μm) of RBCs (red) and EVs (gray) in the CV.

(E) Examples of individual EVs rolling (left) or arresting (right) in the circulation of the CV.

(F) Schematic representation of Zmel1 cells expressing Syntenin2-GFP.

(G) EVs isolated from Zmel1 Syntenin2-GFP cells and labeled with MemBright; the diagram indicates the colocalization between GFP and MemBright (mean and standard deviation).

(H) Temporal projection of a time-lapse of *Tg(Fli:Gal4, UAS:RFP)* embryos injected with Zme1 Syntenin2-GFP EVs imaged immediately after injection.

(I) *Z*-projection of *Tg(Fli:Gal4, UAS:RFP)* embryos injected with Zme1 Syntenin2-GFP EVs imaged 1h after injection.

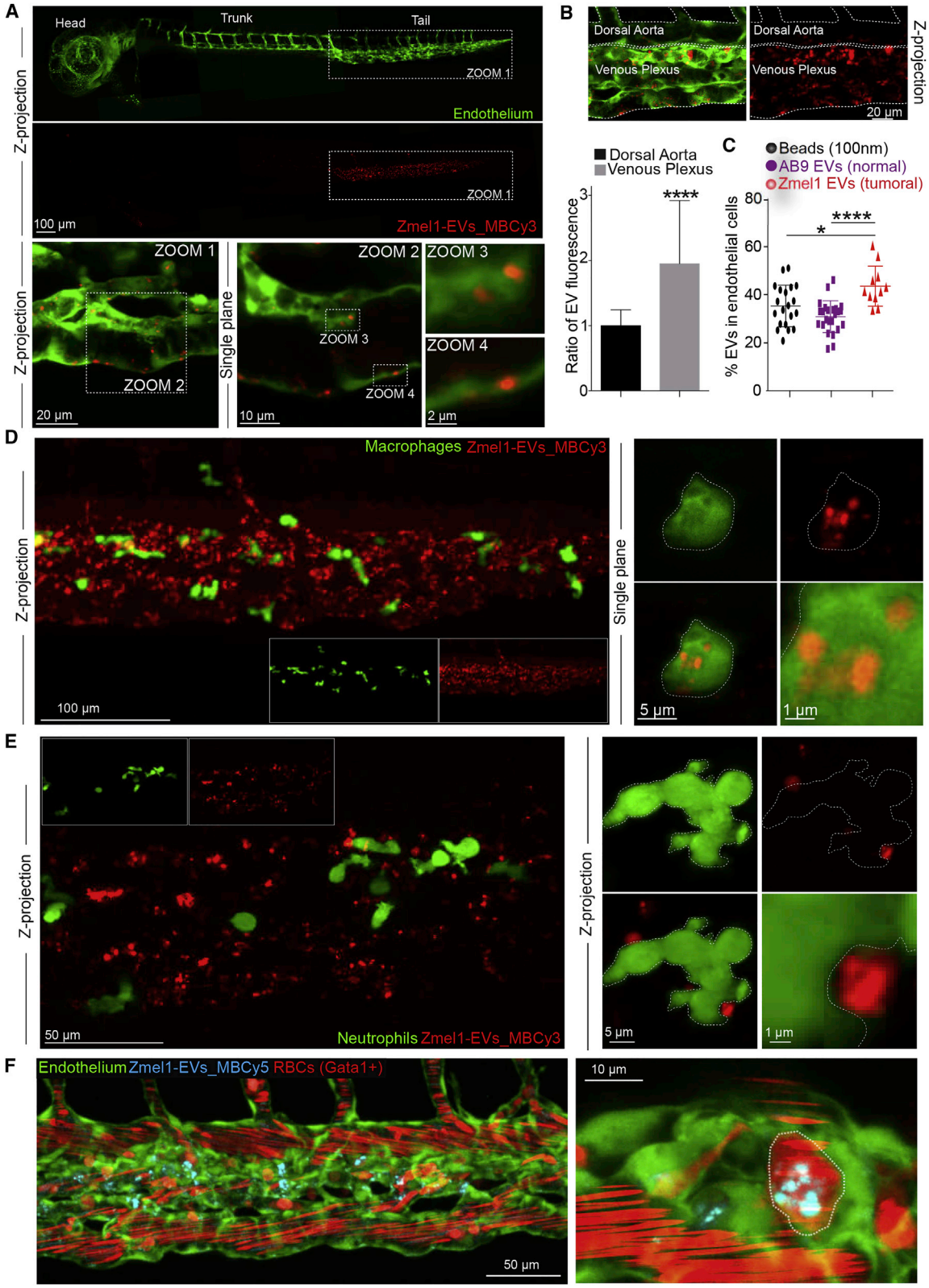

Figure 4. Zmel1 EVs Are Mainly Taken Up by Endothelial Cells, Macrophages, and Hematopoietic Stem Cells but Not by Neutrophils

(A) Confocal images of MemBright-Cy3 labeled Zmel1 EVs 3 h post-injection (hpi) in *Tg(Fli1:GFP)* embryos (endothelium specific expression). The upper panels were stitches from several individual images to allow a large region to be visualized.

(legend continued on next page)

EVs can be tracked in the bloodstream of zebrafish embryos, allowing the study of their hemodynamic behavior and intravascular arrest.

Circulating Tumor EVs Are Mostly Taken Up by Endothelial Cells and Patrolling Macrophages

How circulating tumor EVs target specific cell types at distance remains a mystery, mostly because this step could not be captured before. Here, most of the tumor EVs are found arrested, exclusively in the tail region of the fish, only 10 to 15 min following injection (Figure 4A). In addition, we found that most of the uptake by endothelial cells occurs in the venous region (Figure 4B), suggesting that the permissive flow profiles of this particular region favor arrest and uptake of tumor EVs, as they do for circulating tumor cells (Follain et al., 2018a). Syntenin2-GFP EVs arrest similarly in *Tg(Fli:Gal4, UAS:RFP)* embryos (Figure 3I) and similar observations have been done for endogenous EVs (Verweij et al., 2019). To assess which cell types could uptake tumor EVs, we used four transgenic zebrafish lines with different tissue-specific fluorescent expression *Tg(Fli1:GFP)* for the endothelium (Figure 4A), *Tg(mpeg1:GFP)* for macrophages (Figure 4D), *Tg(mpo:GFP)* for neutrophils (Figure 4E), and *Tg(gata1:dsRed)* for RBCs and putative hematopoietic stem cells (Figure 4F). We found that tumor EVs are rapidly taken up by endothelial cells, macrophages, and immobile Gata1-positive cells (putative hematopoietic stem cells) but not by neutrophils that are known to have a reduced phagocytic activity (Figures 4A, 4D, 4E, and 4F) (Le Guyader et al., 2008). Embryos injected with the MemBright dye alone do not show any signal that could arise from soluble fluorescent aggregates (Figure S3). In addition, endothelial cells and macrophages take up equivalent proportions of Zmel1 EVs, 43% (n = 19 fish) and 38% (n = 11) respectively. Together, this represents the large majority of arrested EVs in the zebrafish embryo at that stage. Importantly, a similar behavior is observed for endogenous CD63-positive EVs (Verweij et al., 2019), suggesting again that circulating EVs of different origins share common mechanisms of arrest *in vivo*. Interestingly, although inert polystyrene beads and non-tumoral EVs (from AB9 zebrafish fibroblasts) can be taken up by macrophages and endothelial cells, they show a reduced accumulation compared to Zmel1 EVs (Figures 4C and 5C). This suggests that both unspecific and specific uptake mechanisms co-exist *in vivo*.

In mice, tumor EVs are internalized by different types of monocytes and macrophages (Whiteside, 2016). In the zebrafish embryo, we noticed that tumor EVs are mostly taken up by small round mpeg1-positive cells (Figures 5A and 5B). In non-injected embryos, these round cells are in direct contact with the blood flow (Figure 5A), which they scan using long protrusions (Figure 5D; Video S3). They also display a reduced velocity (Figure 5E; Video S4). Therefore, the morphology, location, and dynamics of these cells are reminiscent of patrolling monocytes, which are known to play an important role in tumor progression and metastasis in mice and humans (Auffray et al., 2007; Carlin et al., 2013; Hanna et al., 2015). To confirm this observation and gain insight into the ultrastructure of these cells, we used our established CLEM procedure (Goetz et al., 2014; Karreman et al., 2016b) in *Tg(mpeg1:GFP)* embryos injected with tumor EVs labeled with MemBright-Cy3 (Figure 5F; Video S5). We targeted two typical mpeg1:GFP positive cells that have taken up circulating tumor EVs in the living zebrafish embryo (see STAR Methods; Figures S4A and S4B). Fine segmentation of EM images revealed that macrophages localize in a cavity of the lumen of the vessel, where they form tight contacts with the endothelium and extend wide protrusions in the lumen (Figure 5F; Video S5). Interestingly, the region of the endothelium that contacts the macrophages is enriched of endocytic structures, suggesting active exchange between those two cell types (Figure 5G). The macrophages that have taken up tumor EVs extend long and dynamic protrusions in the lumen of the vessel (Figures 5D and 5H), as shown for patrolling monocytes in mice (Carlin et al., 2013). Surprisingly, analysis of the serial sections reveals that their height can be >3 μm and that these protrusions are actually forming large flat sheets deployed in the lumen. Altogether, our data show that circulating tumor EVs are rapidly taken up by patrolling macrophages in the zebrafish embryo, which suggests that it can be used to track the mechanisms of delivery of tumor EVs at high spatiotemporal resolution.

Internalized Tumor EVs Are Targeted to Late Endosomal Compartments

To gain further insight into the mechanisms through which patrolling macrophages uptake tumor EVs, we then imaged the dynamics of circulating tumor EVs (Video S6A). On one hand, EVs arrest at the surface of the macrophage and undergo a slow internalization that can be tracked at optimal spatiotemporal resolution (Figures 6A and 6C; Video S6B). The timing of this uptake (∼ 30 s) is in the range of classical endocytosis (Figure 6A) (Idrissi and Geli, 2014; Taylor et al., 2011). On the other hand, tumor EVs are first caught by a protrusion extending from the macrophage, and then crawl back toward the cell center before being internalized at the basis of the protrusion (Figures 6B and 6C; Video S6C). This second mechanism of internalization is significantly faster (< 5 s) (Figure 6C).

Next, we wondered which intracellular compartments are targeted by uptaken EVs. For this, we incubated *Tg(mpeg1:GFP)* zebrafish embryos with the LysoTracker to label late endosome-lysosomes (LELs). Rapidly after injection, several Zmel1 EVs already colocalize with LysoTracker, although the majority does not (Figure 6D). This colocalization increases over time and 3 h post-injection (hpi), most EV signal is found in

(B) *Z*-projections showing the borders of the dorsal aorta (DA) and the venous plexus (VP), and a histogram showing the EV fluorescence per surface in DA and VP (mean and standard deviation; $p < 0.0001$; Mann-Whitney test).

(C) Quantification of the proportion of 100 nm polystyrene beads, fibroblasts AB9 Evs, or Zmel1 melanoma EVs taken up by endothelial cells 3 hpi (Zmel1 EVs Vs beads: $p = 0.015$, unpaired t test; Zmel1 EVs Vs AB9 EVs: $p < 0.0001$, unpaired t test).

(D) Confocal images of MemBright-Cy3 labeled Zmel1 EVs 3 hpi in *Tg(mpeg1:GFP)* (macrophage specific expression).

(E) Confocal images of MemBright-Cy3 labeled Zmel1 EVs 3 hpi in *Tg(mpo1:GFP)* (neutrophil-specific expression).

(F) Confocal images of MemBright-Cy5 labeled Zmel1 EVs 3 hpi in *Tg(Fli1:GFP; Gata1:RFP)* (GFP: endothelium; *Gata1*: red blood cells and hematopoietic stem cells).

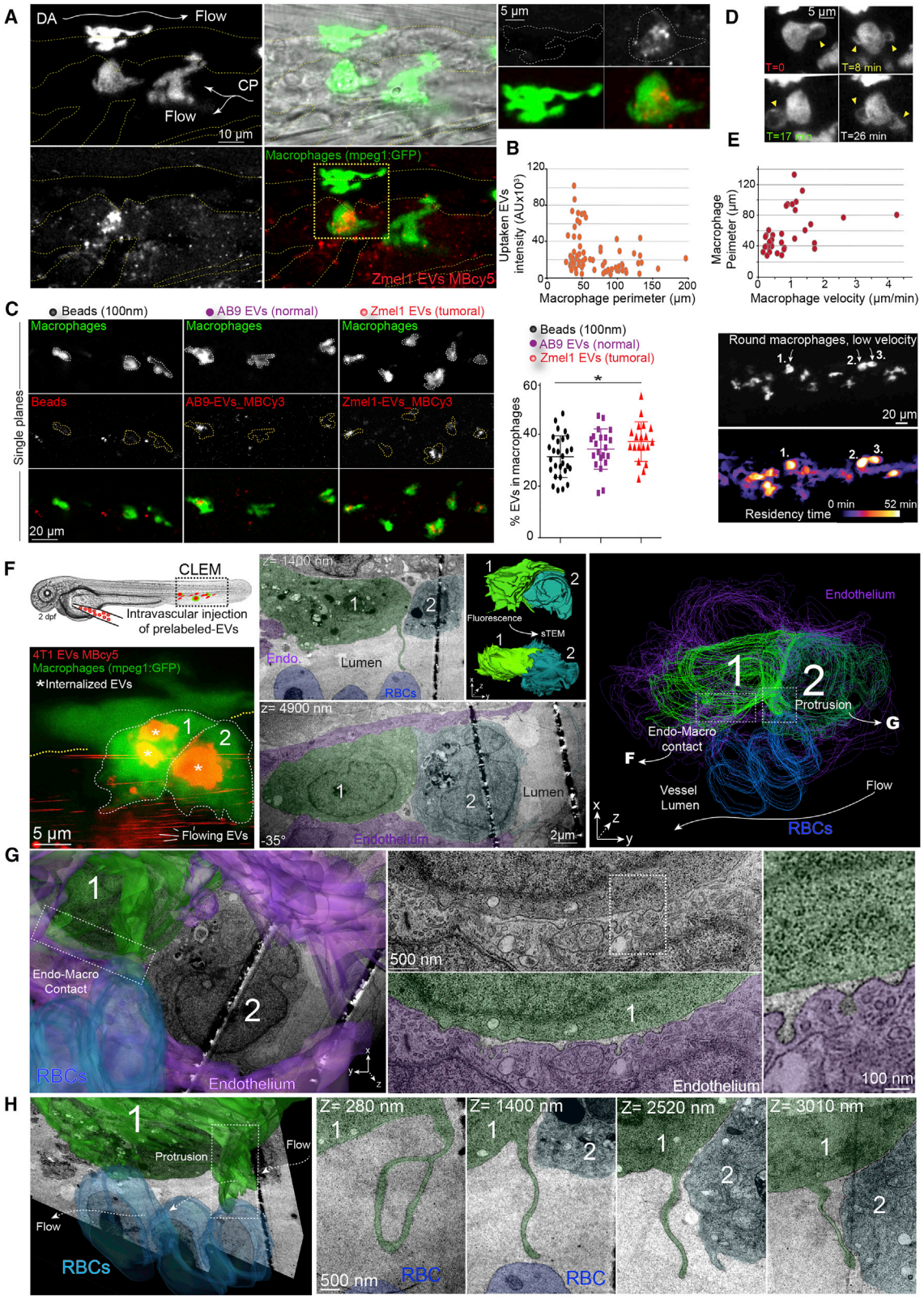

Figure 5. Circulating EVs Are Taken Up by Patrolling Macrophages

(A) Confocal Z projection images of MemBright-Cy3 labeled Zmel1 EVs injected in *Tg(mpeg1:GFP)* (left) with zoom on elongated macrophages devoid of EVs and round macrophages accumulating EVs (right).

(legend continued on next page)

endosome-lysosome compartments (Figure 6D). Of note, 24 hpi, the MemBright signal is still visible and fully colocalizes with LysoTracker (Figure 6D). Although this approach provides a dynamic view of EVs trafficking in zebrafish embryos, LysoTracker labeling does not distinguish between MVBs, late endosomes, and lysosomes. To complement this study, we again exploited our established CLEM procedure on *Tg(mpeg1:GFP)* embryos injected with tumor EVs (Figures 5F–5H and 6E). We generated a 3D model of MemBright-labeled EVs in each macrophage, based on the confocal fluorescent data (called fluorescent 3D model, Figure 6F, upper panel). In parallel, based on TEM serial sections of the same cells, we segmented all the MVBs, late endosomes, and lysosomes that we could locate, and generated a 3D model of these compartments (called TEM 3D model) (Figure 6F, lower panel; Video S5). When comparing the two models, we found that the 3D model created from the fluorescent tumor EVs overlaps with the model from serial TEM sections of LELs (Video S5). This suggests that the internalized tumor EVs are stored within these MVBs, LELs compartments that we imaged at high-resolution (Figure 6E, lower panels). Besides, close examination of the EM stack revealed EVs present in the lumen of the vessel, in close proximity of macrophage protrusions, as well as putative EVs present in endosomes (Figures S4C–S4E). Altogether, this demonstrates the power of the zebrafish embryo to track, at multiple scales, the fate of nanometer-sized objects such as tumor EVs.

Tracking the Release of EVs *In Vivo* Using MB and Genetically Engineered Cells

We focused so far on tumor EVs that were previously isolated and labeled *in vitro* and subsequently tracked *in vivo*. This strategy, however, does not allow tracking of tumor EVs shed from *in-vivo*-grown tumors. Interestingly, we noticed that EVs can be labeled by incubating the secreting cells with the MemBright dye. MemBright quickly and exclusively accumulates in late endosomal compartments of Zmel1 cells in culture (Figure 7A). Upon extensive washing, these cells release fluorescently labeled EVs (Figure 7B) whose morphologies and diameters are similar to EVs from non-labeled cells (Figure 7B). When this approach was used on 4T1 cells expressing CD63-GFP, we could detect EVs positive for both MemBright and CD63, proving that the MemBright can label exosomes (Figure S5). We observed puncta positive for CD63-GFP but not for MemBright and vice-versa. This suggests that the MemBright dye does not label all EVs equally and illustrates the heterogeneity of EVs, which has recently been described (Kowal et al., 2016). Altogether, these experiments suggest that the MemBright is rapidly endocytosed, targeted to MVBs, and incorporated into the membrane of intra-luminal vesicles before being subsequently released outside of the cells attached to the membrane of exosomes. Such a behavior is extremely useful since it allows labeling and tracking of naturally released EVs by pre-incubating cells with MemBright. To prove this, we co-cultured Zmel1 pre-labeled with MemBright-Cy5 with Zmel1 cells expressing cytoplasmic tdTomato. After a week, we observed several Cy5 fluorescent puncta accumulating in the cytoplasm of Zmel1 tdTomato cells, suggesting that indirectly labeled EVs successfully transferred between neighboring cells (Figure 7B). Such a result opens the door to *in vivo* experiments where pre-labeled tumor cells would be grafted in zebrafish embryos (Figures 7C and 7D). To test local EVs transfer, tdTomato Zmel1 cells were pre-labeled with MemBright-Cy5 and subsequently injected into the circulation of *Tg(mpeg1:GFP)* zebrafish embryos. We observed macrophages crawling around arrested Zmel1 tumor cells, and containing Cy5-positive fluorescent puncta (Figure 7C; Video S7), suggesting local EVs transfer between tumor cells and macrophages. These puncta are negative for tdTomato, revealing a different mechanism than the transfer of cytoplasmic material between melanoma cells and macrophages (Roh-Johnson et al., 2017). In addition, we tested the distant transfer of EVs by injecting tdTomato Zmel1 cells pre-labeled with MemBright-Cy5 in the yolk region and imaging macrophages present in the caudal plexus. Similar to the previous experiment, we detected Cy5 fluorescence in macrophages, suggesting the existence of a distant transfer of EVs that exploits the blood circulation for shedding and targeting at distance (Figure 7D). We further validated the ability to detect secreted EVs *in vivo* by intravascular injection of Syntenin2-GFP expressing Zmel1 cells. Upon injection of these cells in the bloodstream, we followed successful extravasation and metastatic outgrowth overtime, which was accompanied by an increased secretion of tumor EVs. While the release of fluorescent EVs was not observed around recently extravasated cells (4 hpi), growing metastatic foci gradually released increasing amounts of Syn2-GFP EVs, which were either mobile or immobile (Figure 7E). Altogether, these experiments demonstrate that the zebrafish embryo allows tracking of the release and transfer of chemically and genetically labeled EVs from tumor to stromal cells *in vivo*.

Tumor EVs Activate Macrophages and Promote Metastatic Growth in Zebrafish

In contrast to inert objects, tumor EVs are loaded with signaling molecules that are likely to affect the fate or behavior of cells that

(B) EVs are mostly taken up by small macrophages. Histogram showing the intensity of taken up EVs (y axis, arbitrary units) versus the perimeter of the macrophages (x axis, μm). Each dot represents one macrophage.

(C) Macrophages internalize tumor EVs more efficiently than 100 nm polystyrene beads (mean and standard deviation; p = 0.016, unpaired t test).

(D) Individual time points of single plane confocal images showing the dynamics of the protrusions in round macrophages.

(E) Histogram showing the perimeter of macrophages (y axis, μm) versus their velocity (x axis, μm/s) (left) and images at the beginning (T = 0) and the end (T = 60 min) of a representative time-lapse. Velocities of migration of *Tg(mpeg1:GFP)*-positive cells are represented with a color code. Three round *Tg(mpeg1:GFP)*-positive cells (1, 2, and 3) show very little displacement during one h.

(F) CLEM experiment on *Tg(mpeg1:GFP)* embryos injected with MemBright-Cy3 4T1 EVs imaged by confocal right after injection (left, *Z* projection). Middle: electron microscopy images on two different *Z* planes showing the same cells. Right: 3D model showing the two macrophages (green), the endothelium (purple), and three red blood cells (blue).

(G) Electron microscopy images of the contact between the endothelium and the macrophage, showing the accumulation of endocytic structures on the endothelium side.

(H) 3D model and electron microscopy images of one protrusion sent by the macrophage into the lumen. This protrusion is visible over several microns in Z.

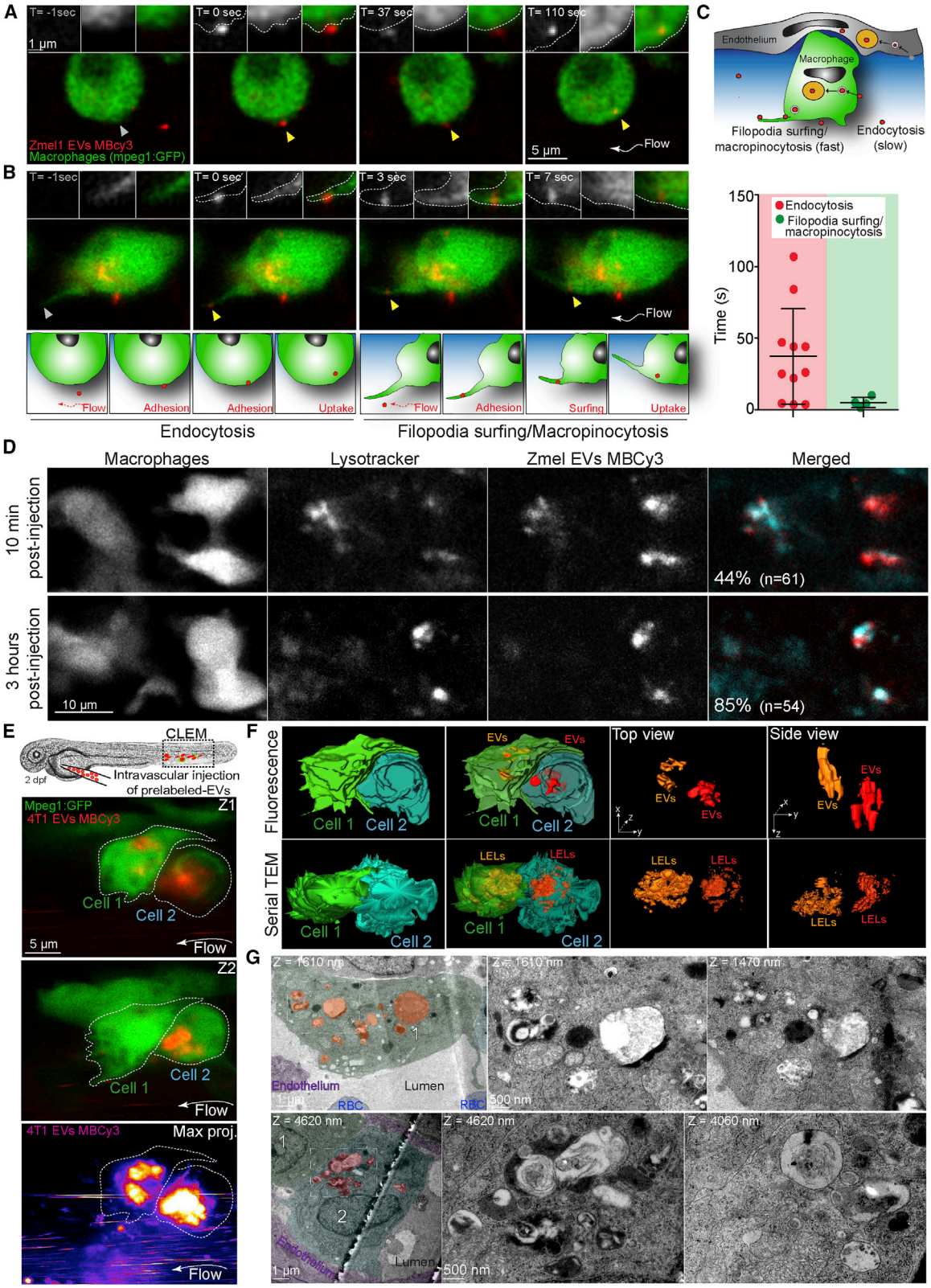

(legend on next page)

internalize them. We thus assessed whether Zmel1 EVs could modify the behavior of receiving cells. We focused on macrophages, which are taking up most of the circulating EVs, and first analyzed their velocities upon uptake. The uptake of tumor EVs by patrolling macrophages significantly reduced their motility when compared to macrophages that had internalized control beads (Figure 8A). Since macrophage velocity has been associated with their activation status *in vitro* (Vogel et al., 2014), we chose to evaluate the impact of Zmel1 EVs on macrophage activation. To do this, we used a recently described transgenic line that relies on the expression of TNF-α to discriminate between pro-inflammatory "M1-like" and "M2-like" polarized macrophages (Nguyen-Chi et al., 2015). Strikingly, most embryos injected with Zmel1 EVs showed M1 activated macrophages 20 hpi (Figures 8B and 8C). Such switches were rarely observed when embryos were injected with 100 nm control polystyrene beads, which clearly demonstrates that circulating Zmel1 EVs can modify the behavior of receiving cells at distance. Tumor EVs can educate receiving cells and confer them pro-metastatic characteristics (Peinado et al., 2017). Inspired by such experiments mostly performed in mice, we next assessed whether circulating tumor EVs could tune metastatic outgrowth. We first "primed" embryos with intravascular injection of either Zmel1 EVs (or 100 nm polystyrene beads). After 12 h, the same embryos were injected with Zmel1 cells in a classical experimental metastasis assay as previously performed (Follain et al., 2018a). Metastatic growth was assessed 7 days later by measuring fluorescence in the caudal plexus. We observed a marked and significant increase in metastatic outgrowth when embryos were primed with Zmel EVs, and not with inert beads (Figure 8D). Furthermore, metastatic foci of embryos primed with tumor Zmel EVs were strikingly more invasive and displayed colonization of the fin parenchyma (Figures 8D and 8E). Altogether, these experiments demonstrate that (1) tumor EVs transform the phenotypes of macrophages and (2) favor metastatic outgrowth and invasiveness by modifying the microenvironment. In addition to demonstrating that labeling EVs with MemBright does not perturb their function, this further validates the use of zebrafish embryos to dissect, with high spatiotemporal resolution, the cascade of events induced by circulating tumor EVs and leading to pre-metastatic niche formation *in vivo*.

DISCUSSION

The work presented here establishes the zebrafish embryo as a new animal model to study tumor EVs *in vivo*. It demonstrates the proximity of zebrafish melanoma EVs to human melanoma EVs and shows how a new membrane probe, the MemBright, specifically and brightly labels EVs. Using this probe, but also genetically labeled EVs, we were able to precisely track their fate and behavior at high spatiotemporal resolution *in vivo*. This allowed us to provide a description of the behavior of tumor EVs circulating in the blood flow and to track their fate upon arrest. We identify the three main cell types taking up circulating tumor EVs (endothelial cells, patrolling macrophages, and putative hematopoietic stem cells) and unravel their uptake mechanisms. Besides, we describe two complementary methods, a conventional genetic approach and the pre-labeling of secreting cells by MemBright, allowing to track the release and transfer of EVs *in vivo*. Finally, we provide evidence for a functional role of tumor EVs in altering the metastatic microenvironment and promoting metastatic outgrowth in zebrafish embryos.

In a parallel study, Verweij and colleagues examine the fate of CD63 positive EVs secreted by the YSL in zebrafish embryo (Verweij et al., 2019). They track endogenous EVs, genetically labeled and naturally secreted during zebrafish development, while we tracked exogenous MemBright-labeled injected tumor EVs. Yet, both studies reach similar conclusions. They both show that (1) endogenous and tumor EVs mainly arrest in the caudal plexus, in regions of low blood flow, (2) EVs are mostly taken up by endothelial cells and patrolling macrophages, and (3) EVs are stored in acidic compartments. Together, our reports establish the zebrafish embryo (*Danio rerio*) as a new model to study fundamental aspects of EVs biology *in vivo*. It thus represents a precious and complementary tool to invertebrate models *Drosophila* and *C. elegans*, which already contributed to better understand the mechanisms of EV secretion as well as their function (Beer and Wehman, 2017).

In addition, we propose the zebrafish embryo as a new and complementary model to murine and human cell culture systems for studying the fate and the function of tumor EVs during the priming of metastatic niches at distance. Compared to *in vitro* systems, zebrafish embryo offers an invaluable complex microenvironment, where different cell types known to contribute to tumor progression are present and can be tracked using established fluorescent transgenic lines. Its transparency allows visualization of individual tumor EVs dispersion and uptake in living zebrafish with unprecedented spatiotemporal resolution, which represents a major advantage over the mouse, where more complex intravital imaging procedures are required in order to visualize single EVs (Lai et al., 2015; Van Der Vos et al., 2016; Zomer et al., 2015). The zebrafish embryo is also amenable to CLEM,

Figure 6. EVs Are Taken Up through Different Mechanisms and Accumulate in Late Endosomal Compartments

(A and B) Single-plane confocal images of *Tg(mpeg1:GFP)* embryos injected with Zmel1 MemBright-Cy3 (MBCy3) EVs extracted from time-lapses generated immediately after injection and showing: (A) the attachment and uptake of EVs by endocytosis and (B) the sliding of EVs on the macrophage protrusion and its fast internalization.

(C) Schematic representation of the modes of uptake by macrophages (upper) and histogram showing the duration (y axis, s) of those two mechanisms (mean and standard deviation).

(D) Single plane confocal images of *Tg(mpeg1:GFP)* embryos injected with Zmel1 MBCy3 EVs and incubated with LysoTracker.

(E) CLEM experiment on *Tg(mpeg1:GFP)* embryos injected with MemBright-Cy3 4T1 EVs imaged by confocal (2 single confocal planes of the GFP and the MBCy3 channels and Z projection of the EV channel (lower)).

(F) 3D model of the two cells and the taken up EVs generated from the confocal data (upper panel, fluorescence), and 3D model of the two cells and the MVBs-late endosomes-lysosomes compartments (LELs) generated from the serial transmission electron microscopy data (lower panel, serial TEM).

(G) Global view of each macrophage highlighting the MVBs-late endosomes-lysosomes compartments (orange and red, left). Zooms of those compartments are shown on the right in two different *Z* positions of the same region.

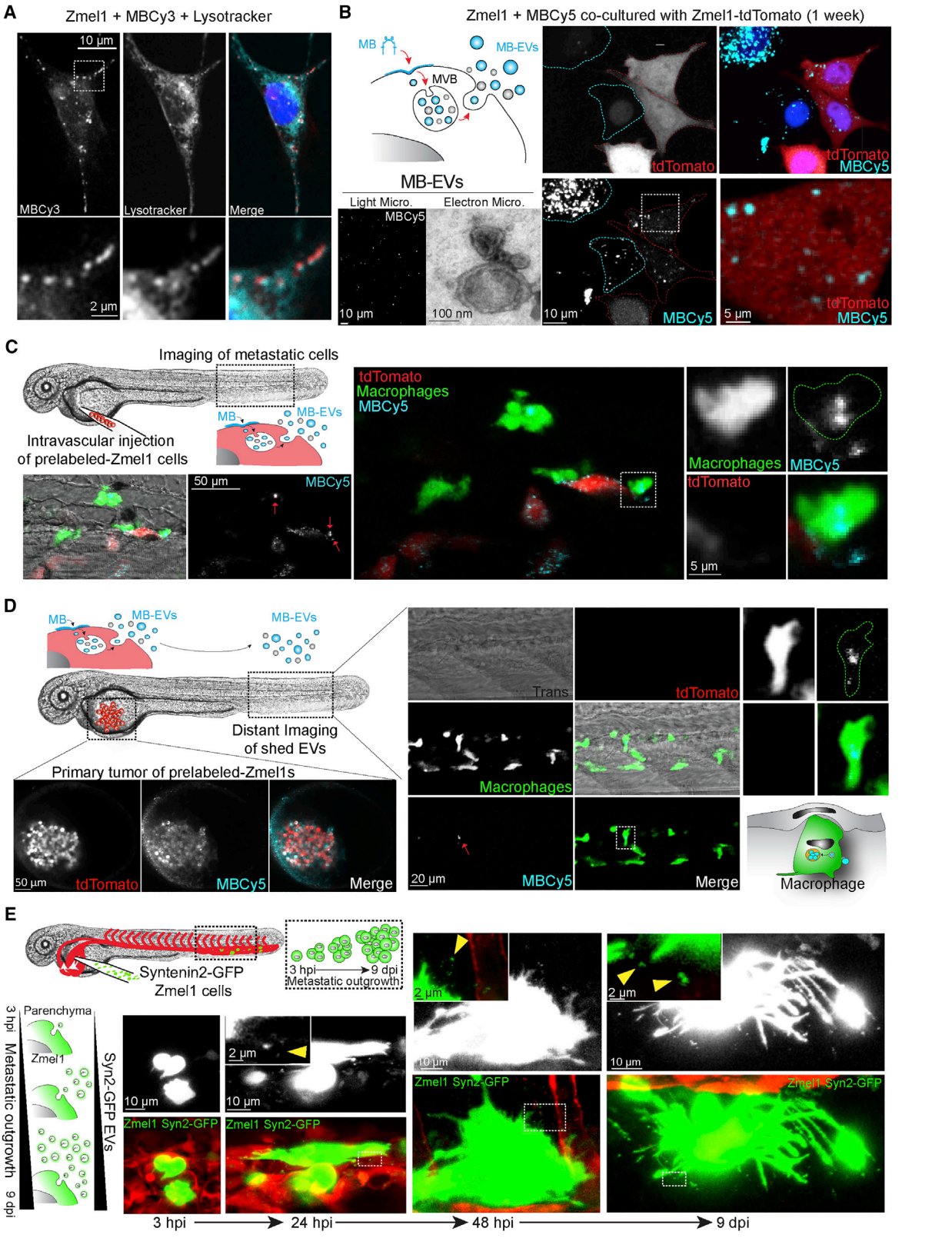

(legend on next page)

through procedures which are simplified compared to the mouse (Goetz et al., 2015; Karreman et al., 2016b). In the future, nanoscale imaging should unravel how tumor EVs secreted by a primary tumor reach the blood circulation before crossing the endothelium when reaching a given organ but also to grasp the details of their uptake and trafficking at a subcellular level.

Here, we show that most tumor EVs are internalized by a subset of macrophages. We consider these cells as functionally similar to murine and human patrolling monocytes for the following reasons: (1) they are positive for the mpeg1 promoter, which is expressed both by monocytes and macrophages in human (Spilsbury et al., 1995), (2) they are small, round and have a slow migration velocity when compared to elongated differentiated macrophages, and (3) they are sending highly dynamic protrusions toward the lumen of the vessels and show areas of direct cell-cell contacts with the endothelial wall, as previously shown (Murayama et al., 2006). These last two aspects match the main characteristics of human and mice patrolling monocytes (Auffray et al., 2007; Carlin et al., 2013). Notably, CLEM analysis reveals that the dynamic protrusions observed in live imaging are actually flat sheets of several microns that scan the vessel lumen and could function as butterfly nets to catch tumor EVs deep in the vessel lumen. Such structures are specific to macrophages, allowing them to internalize fluid-borne objects, unlike neutrophils that only phagocytose surface-bound ones (Colucci-Guyon et al., 2011). Once they have contacted the protrusion, the EVs quickly slide toward the cell body through unknown mechanisms, which could be similar to the filopodia surfing recently described (Heusermann et al., 2016). Those protrusions could also participate in macropinocytic uptake of EVs, similar to what has been observed by microglia (Fitzner et al., 2011). EVs are then internalized at the basis of the protrusions, probably in regions of active endocytosis. Interestingly, our EM data revealed several EVs present at the basis of protrusions (see Figure S4C). Alternatively, circulating EVs can directly bind to the macrophage surface before being endocytosed. The capacity of patrolling macrophages to rapidly uptake circulating EVs explains the very short half-life (10–20 min) of circulating EVs after their injection in the blood circulation of either mouse (Morishita et al., 2015; Saunderson et al., 2014; Takahashi et al., 2013) or zebrafish (our work). This is in agreement with the observation that chemical depletion of monocytes and macrophages in mice dramatically increases the stability of circulating EVs (Imai et al., 2015).

Tumor EVs are then rapidly stored in acidic degradative compartments, similar to what has been described for macrophages *in vitro* (Feng et al., 2010). Determining whether and how internalized EVs deliver signaling molecules to the receiving cell, although they are mostly targeted to degradative compartments, is a central question in the EV field. It will be particularly important to address it in the case of tumor EVs taken up by patrolling macrophages. It is interesting to note that uptake mechanisms and compartments are similar between exogenous tumor EVs (this study) and endogenous EVs (Verweij et al., 2019). This suggests that tumor EVs are internalized using universal mechanisms and further demonstrates that the zebrafish embryo is a perfect model for dissecting such behavior.

In addition, the zebrafish embryo allows a direct comparison of EVs with distinct sizes, contents, or origins. This will be essential to better understand the heterogeneity of EVs, as it is now clear that multiple sub-populations (or sizes) of EVs co-exist with different cargo contents and presumably different functions (Kowal et al., 2016). Co-injection of different types of EVs can, for instance, be used to precisely dissect the involvement of one given EV transmembrane or cargo protein, or to compare tumor EVs from patients at different stages of tumor progression. Using multi-color MemBright probes (Cy3, 5, or 7) to label EVs, it is possible to directly compare the behavior of co-injected populations of EVs. Labeling EVs with membrane probes after their isolation is fast and allows obtaining bright fluorescent EVs regardless of their origin. It is particularly relevant for EVs isolated from cell lines reluctant to gene expression manipulation, from animal body fluids, or, importantly, in the case of tumor EVs from samples of cancer patients. However, the use of membrane probes requires the assurance of labeling specificity. This is particularly essential for studies aiming to track EVs dispersion and uptake, as dye aggregates can easily be confounded with EVs, due to their small sizes (Lai et al., 2015; Takov et al., 2017). Here, using spectroscopic and microscopic approaches, we have shown that the MemBright does not form such fluorescent aggregates, in contrast to commonly used PKH. In addition, it is brighter and can therefore be used at reduced concentrations, minimizing again the risk of false-positive results. The key difference of MemBright from PKH is the presence of amphiphilic groups, which favor efficient transfer of the fluorophore from aqueous media to lipid membranes (Collot et al., 2015; Kucherak et al., 2010). Therefore, MemBright can be used to confidently track EV dispersion and uptake.

Finally, our work demonstrates that zebrafish can be used to dissect the causal relationship between circulating tumor EVs uptake and formation of metastatic niches. While most studies performed in mice demonstrate correlations between bulk injection of EVs and emergence of a pre-metastatic niche, the zebrafish embryo, by allowing continuous imaging, allows direct

Figure 7. Tracking EVs Released by Zebrafish Melanoma Cells

(A) Confocal images of Zmel1 cells incubated with MemBright-Cy3 and stained with LysoTracker.

(B) Schematic representation of the experimental procedure: MemBright added to cells in culture accumulates in MVBs and is subsequently released in exosomes. Such EVs can be observed by electron microscopy. Confocal images of Zmel1 cells pre-labeled with MemBright-Cy5 and co-cultured with Zmel1 tdTomato cells, showing the transfer of MemBright in *Z* projections (left) and single planes (right).

(C) Confocal images of tdTomato Zmel1 cells pre-labeled with MemBright-Cy5 injected in the circulation of *Tg(mpeg1:GFP)* embryos and imaged in the caudal plexus two days post-injection, showing the local transfer of MemBright-Cy5 to macrophages.

(D) Confocal images of tdTomato Zmel1 cells pre-labeled with MemBright Cy5 injected above the yolk of *Tg(mpeg1:GFP)* embryos and imaged in the yolk region (primary tumor, left) and in the caudal plexus (distant imaging of shed EVs, right) two days post-injection, showing the long distance transfer of MemBright-Cy5 to macrophages.

(E) *In vivo* release of Syntenin2-GFP EVs. Zmel1 Syntenin2-GFP cells injected in the circulation of *Tg(Fli:Gal4, UAS:RFP)* embryos and imaged by confocal in the following days.

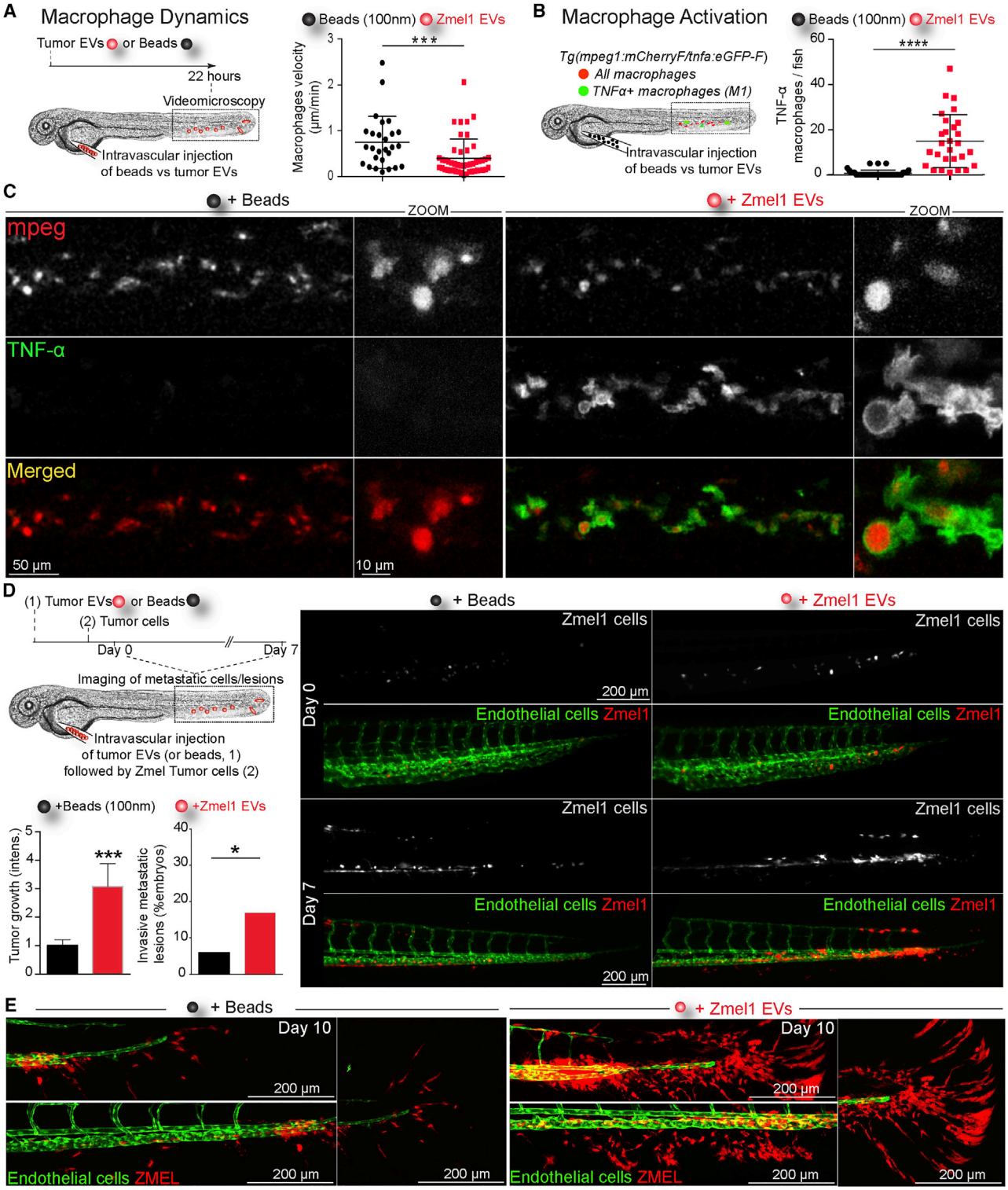

Figure 8. Melanoma EVs Activate Macrophages and Promote Tumor Growth in Zebrafish

(A) 22 h following injection of Zmel1 EVs or 100 nm beads, the dynamics of mpeg1:GFP macrophages was measured by time-lapse. Histogram showing that the velocity of macrophages 22 h after injection (one dot represents one macrophage; mean and standard deviation; p = 0.0009, Mann-Whitney test).

(B) *Tg(mpeg1:mCherry/TNFa:eGFP)* injected with Zmel1 EVs or 100 nm beads and imaged 20 h post-injection. Histogram showing the number of TNFa:GFP positive cells per fish caudal plexus (one dot represents one embryo; mean and standard deviation; p < 0.0001, Mann-Whitney test).

(C) Confocal images of *Tg(mpeg1:mCherry/TNFa:eGFP)* injected with Zmel1 EVs or 100 nm beads and imaged 20 h post-injection.

(legend continued on next page)

quantitative assessment of how metastatic niches are formed and how they can contribute to metastatic outgrowth. In this work, we show that injection of tumor EVs in the circulation is rapidly followed by expression of TNFα, reminiscent of their activation into a pro-inflammatory "M1-like" phenotype. These results are consistent with *in vitro* studies showing that EVs from breast cancer cells or oral squamous carcinoma cells stimulate an M1 macrophage inflammatory response (including TNF induction) (Xiao et al., 2018; Chow et al., 2014). Other studies, however, show that tumor EVs, for instance from prostate tumors, induce an M2 activation (Halin Bergström et al., 2016). Although the M1/M2 binary polarization model of macrophages has been challenged (Aras and Zaidi, 2017), pro-inflammatory macrophages have been reported to exert pro- or anti-tumoral effects depending on the context (Engblom et al., 2016). Further work is thus needed to better understand how tumor EVs tune macrophages' fate during metastatic progression. Here, the zebrafish model offers the opportunity to revisit the interactions between tumor EVs, macrophages and other immune cells (and their activation status), and tumor cells during extravasation and metastatic outgrowth. Recent work performed in mice, which exploited intravital imaging, revealed close interactions between tumor cells arrested in the circulation and myeloid cells and the exchange of microvesicles promoting extravasation (Headley et al., 2016). Complementary usage of these two models, based on intravital imaging, is thus likely to bring important insights into how tumor EVs can tune metastatic outgrowth.

Importantly, we show that pre-treatment of zebrafish with Zmel1 tumor EVs enhances metastatic outgrowth, leading to a more invasive phenotype. This phenotype is reminiscent of several mice studies showing that pre-injection of EVs from either melanoma, pancreatic ductal adenocarcinoma, or breast tumors promotes metastasis of their respective tumors cells injected in the circulation (Costa-Silva et al., 2015; Hoshino et al., 2015; Plebanek et al., 2017). In Zmel1 EVs pre-treated fish, we also observed that tumor cells were more efficient at actively invading the caudal fin. Such a phenotype could result from increased extravasation efficiency or from EV-mediated increased proliferation. Alternatively, it could arise from tumor EVs that can directly alter the extracellular matrix in pre-metastatic niches (Costa-Silva et al., 2015), or induce the secretion of pro-migratory factors by activated pro-inflammatory macrophages (Xiao et al., 2018).

Altogether, our work on the tracking of exogenous tumor EVs (this study) and of endogenous EVs (Verweij et al., 2019) set the zebrafish embryo as a new and highly attractive *in vivo* model to track EVs at the single EV scale. Interestingly, both studies identified similar mechanisms of transit and uptake for physiological and pathological extracellular vesicles, which further validate the zebrafish embryo as a reliable animal model for studying the biology of EVs. Finally, we believe that the zebrafish embryo will open new avenues for EV biology, as it offers adapted time and space scales to the study of small organelles *in vivo*.

STAR★METHODS

Detailed methods are provided in the online version of this paper and include the following:

- KEY RESOURCES TABLE
- CONTACT FOR REAGENT AND RESOURCE SHARING
- EXPERIMENTAL MODEL AND SUBJECT DETAILS
  - Zmel1, Zmel1 tdTomato and Zmel1 Syntenin2-GFP
  - AB9 Cells
  - 4T1 Cells and 4T1 CD63-GFP
  - B16-F0, F1 and F10
  - 451-LU, SK-Mel28, SK-Mel147, SK-Mel103, WM35 and WM164
  - Zebrafish
- METHOD DETAILS
  - Cell Line Generation
  - EV Isolation and Analysis
  - Shotgun Proteomics
  - Protein Comparisons
  - MemBright and PKH Labeling of EVs
  - Spectroscopy
  - Fluorescence Correlation Spectroscopy (FCS)
  - MemBright Labeling of Cells
  - Intravascular Injection of Zebrafish Embryo
  - Confocal Imaging and Analysis
  - Semi-automated Method to Determine the Proportion of Internalized EVs
  - Quantification of EVs in Aorta vs Vein Regions
  - Flow Analysis for Red Blood Cells
  - Flow Analysis of EVs
  - EVs and RBCs Distance and Velocity from the Endothelial Barrier
  - Sample Preparation for Correlative Light and Electronic Microscopy of ZF Embryos
- QUANTIFICATION AND STATISTICAL ANALYSIS
  - Statistical Tests
  - Zebrafish Experiments
  - EVs Experiments
- DATA AND SOFTWARE AVAILABILITY

SUPPLEMENTAL INFORMATION

Supplemental Information includes five figures, two tables, and seven videos and can be found with this article online at https://doi.org/10.1016/j.devcel.2019.01.014.

ACKNOWLEDGMENTS

We thank all members of the Goetz Lab for helpful discussions. We are indebted to K. Richter and F. Peri (EMBL, Heidelberg, Germany) as well as to P. Hanns and C. Lengerke (University Hospital Basel, Switzerland) for supplying zebrafish embryos. We are grateful to R. White (MSKCC, New York, USA) for the Zmel1 (native and tdTomato) cells, to Dr. D.C. Bennett (St. George's University of London, U.K.) and Dr. M. Soengas (CNIO, Madrid, Spain) for mammalian melanoma cells, and to P. Zimmerman (CRCM,

(D) Zmel1-tdTomato tumor growth is enhanced in *Tg(Fli1:GFP)* embryos that were pre-injected with Zmel1 EVs. Histograms showing tumor growth at 7 days (left; $p = 0.0004$, Mann-Whitney test) and invasive lesions at 10 days (right; $p < 0.05$; chi-squared test). Epifluorescent images of tumor growth in the caudal plexus, right panels.

(E) Confocal images of tumor cell invasion in embryos.

Marseille, France) for the Syntenin-2 construct. We thank A. Michel (EFS, Strasbourg, France) and C. Spiegelhalter (IGBMC, Illkirch, France) for EM assistance, Y.Schwab for advice during CLEM analysis (EMBL, Heidelberg), E. Guiot and Y. Lutz (IGBMC, Illkirch, France) for advice on confocal imaging, and A. Audfray (Malvern Instruments) for NTA. We thank the CNIO proteomics core for performing the mass spectrometry on mouse and human melanoma EVs. We thank P. Herbomel for critical reading of the manuscript. This work was supported by a fellowship from IDEX (University of Strasbourg) to S.G.; by grants from La Ligue contre le Cancer, Canceropole Grand-Est, INCa (MetaCLEM) and Roche to J.G.G.; and by institutional funds from University of Strasbourg, INSERM, and ANR (to CC, French Proteomics Infrastructure ProFI; ANR-10-INBS-08-03).

AUTHOR CONTRIBUTIONS

V.H. and J.G.G. planned the project. V.H. designed and conducted most of the experiments with contributions from S.G., B.M., G.F., M.J.G-L., and J.B. M.C. synthesized the MemBright and led the spectroscopy experiments, with A.S.K. S.H. designed the automated EV tracking and the EV colocalization analysis. O.L. engineered the fluorescent cell lines. F.De., J.B., and C.C. conducted the mass spectrometry on Zmel1 EVs. A.I.A., S.G.S., and H.P. lead the mass spectrometry analysis on human and mice melanoma EVs. F.V. and G.v.N. generated the mass spectrometry data on AB9 and endogenous zebrafish EVs. N.F. prepared the samples for CLEM and P.M. did the serial sectioning and the microCT. F.Dj. provided the *Tg(mpeg:mCherry,tnf:GFP)* zebrafish line and advised its use. L.M. and I.B. performed image analysis. V.H. and J.G.G. wrote the manuscript with insights from all authors.

DECLARATION OF INTERESTS

The authors declare no competing interests.

Received: March 15, 2018
Revised: October 19, 2018
Accepted: January 10, 2019
Published: February 7, 2019

REFERENCES

Al-Nedawi, K., Meehan, B., Micallef, J., Lhotak, V., May, L., Guha, A., and Rak, J. (2008). Intercellular transfer of the oncogenic receptor EGFRvIII by microvesicles derived from tumour cells. Nat. Cell Biol. *10*, 619–624.

Aras, S., and Zaidi, M.R. (2017). TAMeless traitors: macrophages in cancer progression and metastasis. Br. J. Cancer *117*, 1583–1591.

Auffray, C., Fogg, D., Garfa, M., Elain, G., Join-Lambert, O., Kayal, S., Sarnacki, S., Cumano, A., Lauvau, G., and Geissmann, F. (2007). Monitoring of blood vessels and tissues by a population of monocytes with patrolling behavior. Science *317*, 666–670.

Baietti, M.F., Zhang, Z., Mortier, E., Melchior, A., Degeest, G., Geeraerts, A., Ivarsson, Y., Depoortere, F., Coomans, C., Vermeiren, E., et al. (2012). Syndecan–syntenin–ALIX regulates the biogenesis of exosomes. Nat. Cell Biol. *14*, 677–685.

Baran, J., Baj-Krzyworzeka, M., Weglarczyk, K., Szatanek, R., Zembala, M., Barbasz, J., Czupryna, A., Szczepanik, A., and Zembala, M. (2010). Circulating tumour-derived microvesicles in plasma of gastric cancer patients. Cancer Immunol. Immunother. *59*, 841–850.

Beer, K.B., and Wehman, A.M. (2017). Mechanisms and functions of extracellular vesicle release in vivo-what we can learn from flies and worms. Cell Adh. Migr. *11*, 135–150.

Carapito, C., Burel, A., Guterl, P., Walter, A., Varrier, F., Bertile, F., and Van Dorsselaer, A. (2014). MSDA, a proteomics software suite for in-depth mass spectrometry Data Analysis using grid computing. Proteomics *14*, 1014–1019.

Cardona, A., Saalfeld, S., Schindelin, J., Arganda-Carreras, I., Preibisch, S., Longair, M., Tomancak, P., Hartenstein, V., and Douglas, R.J. (2012). TrakEM2 software for neural circuit reconstruction. PLoS One *7*, e38011.

Carlin, L.M., Stamatiades, E.G., Auffray, C., Hanna, R.N., Glover, L., Vizcay-Barrena, G., Hedrick, C.C., Cook, H.T., Diebold, S., and Geissmann, F. (2013). Nr4a1-dependent Ly6C(low) monocytes monitor endothelial cells and orchestrate their disposal. Cell *153*, 362–375.

Chow, A., Zhou, W., Liu, L., Fong, M.Y., Champer, J., Van Haute, D., Chin, A.R., Ren, X., Gugiu, B.G., Meng, Z., et al. (2014). Macrophage immunomodulation by breast cancer-derived exosomes requires Toll-like receptor 2-mediated activation of NF-κB. Sci. Rep. *4*, 5750.

Collot, M., Kreder, R., Tatarets, A.L., Patsenker, L.D., Mely, Y., and Klymchenko, A.S. (2015). Bright fluorogenic squaraines with tuned cell entry for selective imaging of plasma membrane vs. endoplasmic reticulum. Chem. Commun. *51*, 17136–17139.

Collot, M., Ashokkumar, P., Anton, H., Boutant, E., Faklaris, O., Galli, T., Mély, Y., Danglot, L., and Klymchenko, A.S. (2019). MemBright: a family of red to near-infrared fluorescent membrane probes for advanced cellular imaging and neuroscience. Cell Chem. Biol. *26*, https://doi.org/10.1016/j.chembiol.2019.01.009.

Colombo, M., Moita, C., van Niel, G., Kowal, J., Vigneron, J., Benaroch, P., Manel, N., Moita, L.F., Théry, C., and Raposo, G. (2013). Analysis of ESCRT functions in exosome biogenesis, composition and secretion highlights the heterogeneity of extracellular vesicles. J. Cell Sci. *126*, 5553–5565.

Colucci-Guyon, E., Tinevez, J.Y., Renshaw, S.A., and Herbomel, P. (2011). Strategies of professional phagocytes in vivo: unlike macrophages, neutrophils engulf only surface-associated microbes. J. Cell Sci. *124*, 3053–3059.

Costa-Silva, B., Aiello, N.M., Ocean, A.J., Singh, S., Zhang, H., Thakur, B.K., Becker, A., Hoshino, A., Mark, M.T., Molina, H., et al. (2015). Pancreatic cancer exosomes initiate pre-metastatic niche formation in the liver. Nat. Cell Biol. *17*, 816–826.

Cox, J., Hein, M.Y., Luber, C.A., Paron, I., Nagaraj, N., and Mann, M. (2014). Accurate Proteome-wide label-free quantification by delayed normalization and maximal peptide ratio extraction, termed MaxLFQ. Mol. Cell Proteomics *13*, 2513–2526.

Van Deun, J., Mestdagh, P., Sormunen, R., Cocquyt, V., Vermaelen, K., Vandesompele, J., Bracke, M., De Wever, O., and Hendrix, A. (2014). The impact of disparate isolation methods for extracellular vesicles on downstream RNA profiling. J. Extracell. Vesicles *3*, 1–14.

EV-TRACK Consortium, Van Deun, J., Mestdagh, P., Agostinis, P., Akay, Ö., Anand, S., Anckaert, J., Martinez, Z.A., Baetens, T., Beghein, E., et al. (2017). EV-TRACK: transparent reporting and centralizing knowledge in extracellular vesicle research. Nat. Methods *14*, 228–232.

Engblom, C., Pfirschke, C., and Pittet, M.J. (2016). The role of myeloid cells in cancer therapies. Nat. Rev. Cancer *16*, 447–462.

Feng, D., Zhao, W.L., Ye, Y.Y., Bai, X.C., Liu, R.Q., Chang, L.F., Zhou, Q., and Sui, S.F. (2010). Cellular internalization of exosomes occurs through phagocytosis. Traffic *11*, 675–687.

Fitzner, D., Schnaars, M., van Rossum, D., Krishnamoorthy, G., Dibaj, P., Bakhti, M., Regen, T., Hanisch, U.K., and Simons, M. (2011). Selective transfer of exosomes from oligodendrocytes to microglia by macropinocytosis. J. Cell Sci. *124*, 447–458.

Follain, G., Osmani, N., Azevedo, A.S., Allio, G., Mercier, L., Karreman, M.A., Solecki, G., Garcia Leòn, M.J., Lefebvre, O., Fekonja, N., et al. (2018a). Hemodynamic forces tune the arrest, adhesion, and extravasation of circulating tumor cells. Dev. Cell *45*, 33–52.

Follain, G., Osmani, N., Fuchs, C., Allio, G., Harlepp, S., and Goetz, J.G. (2018b). Using the zebrafish embryo to dissect the early steps of the metastatic cascade. Methods Mol. Biol. *1749*, 195–211.

Galindo-Hernandez, O., Villegas-Comonfort, S., Candanedo, F., González-Vázquez, M.C., Chavez-Ocaña, S., Jimenez-Villanueva, X., Sierra-Martinez, M., and Salazar, E.P. (2013). Elevated concentration of microvesicles isolated from peripheral blood in breast cancer patients. Arch. Med. Res. *44*, 208–214.

Goetz, J.G., Steed, E., Ferreira, R.R., Roth, S., Ramspacher, C., Boselli, F., Charvin, G., Liebling, M., Wyart, C., Schwab, Y., et al. (2014). Endothelial cilia mediate low flow sensing during zebrafish vascular development. Cell Rep. *6*, 799–808.

Goetz, J.G., Monduc, F., Schwab, Y., and Vermot, J. (2015). Using correlative light and electron microscopy to study zebrafish vascular morphogenesis. Methods Mol. Biol. *1189*, 31–46.

Grange, C., Tapparo, M., Collino, F., Vitillo, L., Damasco, C., Deregibus, M.C., Tetta, C., Bussolati, B., and Camussi, G. (2011). Microvesicles released from human renal cancer stem cells stimulate angiogenesis and formation of lung premetastatic niche. Cancer Res. *71*, 5346–5356.

Gu, J., Qian, H., Shen, L., Zhang, X., Zhu, W., Huang, L., Yan, Y., Mao, F., Zhao, C., Shi, Y., et al. (2012). Gastric cancer exosomes trigger differentiation of umbilical cord derived mesenchymal stem cells to carcinoma-associated fibroblasts through TGF-β/Smad pathway. PLoS One *7*, e52465.

Le Guyader, D., Redd, M.J., Colucci-Guyon, E., Murayama, E., Kissa, K., Briolat, V., Mordelet, E., Zapata, A., Shinomiya, H., and Herbomel, P. (2008). Origins and unconventional behavior of neutrophils in developing zebrafish. Blood *111*, 132–141.

Halin Bergström, S., Hägglöf, C., Thysell, E., Bergh, A., Wikström, P., and Lundholm, M. (2016). Extracellular vesicles from metastatic rat prostate tumors prime the normal prostate tissue to facilitate tumor growth. Sci. Rep. *6*, 31805.

Hanna, R.N., Cekic, C., Sag, D., Tacke, R., Thomas, G.D., Nowyhed, H., Herrley, E., Rasquinha, N., McArdle, S., Wu, R., et al. (2015). Patrolling monocytes control tumor metastasis to the lung. Science *350*, 985–990.

Headley, M.B., Bins, A., Nip, A., Roberts, E.W., Looney, M.R., Gerard, A., and Krummel, M.F. (2016). Visualization of immediate immune responses to pioneer metastatic cells in the lung. Nature *531*, 513–517.

Heilmann, S., Ratnakumar, K., Langdon, E.M., Kansler, E.R., Kim, I.S., Campbell, N.R., Perry, E.B., McMahon, A.J., Kaufman, C.K., Van Rooijen, E., et al. (2015). A quantitative system for studying metastasis using transparent zebrafish. Cancer Res. *75*, 4272–4282.

Heusermann, W., Hean, J., Trojer, D., Steib, E., von Bueren, S., Graff-Meyer, A., Genoud, C., Martin, K., Pizzato, N., Voshol, J., et al. (2016). Exosomes surf on filopodia to enter cells at endocytic hot spots and shuttle within endosomes to scan the ER. J. Cell Biol. *213*, 173–184.

Hoshino, A., Costa-Silva, B., Shen, T.L., Rodrigues, G., Hashimoto, A., Tesic Mark, M., Molina, H., Kohsaka, S., Di Giannatale, A., Ceder, S., et al. (2015). Tumour exosome integrins determine organotropic metastasis. Nature *527*, 329–335.

Hyenne, V., Lefebvre, O., and Goetz, J.G. (2017). Going live with tumor exosomes and microvesicles. Cell Adh. Migr. *11*, 173–186.

Idrissi, F.Z., and Geli, M.I. (2014). Zooming in on the molecular mechanisms of endocytic budding by time-resolved electron microscopy. Cell. Mol. Life Sci. *71*, 641–657.

Imai, T., Takahashi, Y., Nishikawa, M., Kato, K., Morishita, M., Yamashita, T., Matsumoto, A., Charoenviriyakul, C., and Takakura, Y. (2015). Macrophage-dependent clearance of systemically administered B16BL6-derived exosomes from the blood circulation in mice. J. Extracell. Vesicles *4*, 26238.

Karreman, M.A., Mercier, L., Schieber, N.L., Solecki, G., Allio, G., Winkler, F., Ruthensteiner, B., Goetz, J.G., and Schwab, Y. (2016a). Fast and precise targeting of single tumor cells in vivo by multimodal correlative microscopy. J. Cell Sci. *129*, 444–456.

Karreman, M.A., Hyenne, V., Schwab, Y., and Goetz, J.G. (2016b). Intravital correlative microscopy: imaging life at the nanoscale. Trends Cell Biol. *26*, 848–863.

Kowal, J., Arras, G., Colombo, M., Jouve, M., Morath, J.P., Primdal-Bengtson, B., Dingli, F., Loew, D., Tkach, M., and Théry, C. (2016). Proteomic comparison defines novel markers to characterize heterogeneous populations of extracellular vesicle subtypes. Proc. Natl. Acad. Sci. USA *113*, E968–E977.

Kucherak, O.A., Oncul, S., Darwich, Z., Yushchenko, D.A., Arntz, Y., Didier, P., Mély, Y., and Klymchenko, A.S. (2010). Switchable Nile red-based probe for cholesterol and lipid order at the outer leaflet of biomembranes. J. Am. Chem. Soc. *132*, 4907–4916.

Lai, C.P., Mardini, O., Ericsson, M., Prabhakar, S., Maguire, C.A., Chen, J.W., Tannous, B.A., and Breakefield, X.O. (2014). Dynamic biodistribution of extracellular vesicles in vivo using a multimodal imaging reporter. ACS Nano *8*, 483–494.

Lai, C.P., Kim, E.Y., Badr, C.E., Weissleder, R., Mempel, T.R., Tannous, B.A., and Breakefield, X.O. (2015). Visualization and tracking of tumour extracellular vesicle delivery and RNA translation using multiplexed reporters. Nat. Commun. *6*, 7029.

Liu, Y., Gu, Y., Han, Y., Zhang, Q., Jiang, Z., Zhang, X., Huang, B., Xu, X., Zheng, J., and Cao, X. (2016). Tumor exosomal RNAs promote lung pre-metastatic niche formation by activating alveolar epithelial TLR3 to recruit neutrophils. Cancer Cell *30*, 243–256.

Logozzi, M., De Milito, A., Lugini, L., Borghi, M., Calabrò, L., Spada, M., Perdicchio, M., Marino, M.L., Federici, C., Iessi, E., et al. (2009). High levels of exosomes expressing CD63 and caveolin-1 in plasma of melanoma patients. PLoS One *4*, e5219.

Magde, D., Rojas, G.E., and Seybold, P.G. (1999). Solvent dependence of the fluorescence lifetimes of xanthene dyes. Photochem. Photobiol. *70*, 737–744.

Morishita, M., Takahashi, Y., Nishikawa, M., Sano, K., Kato, K., Yamashita, T., Imai, T., Saji, H., and Takakura, Y. (2015). Quantitative analysis of tissue distribution of the B16BL6-derived exosomes using a streptavidin-lactadherin fusion protein and iodine-125-Labeled biotin derivative after intravenous injection in mice. J. Pharm. Sci. *104*, 705–713.

Müller, P., Schwille, P., and Weidemann, T. (2014). PyCorrFit - generic data evaluation for fluorescence correlation spectroscopy. Bioinformatics *30*, 2532–2533.

Murayama, E., Kissa, K., Zapata, A., Mordelet, E., Briolat, V., Lin, H.F., Handin, R.I., and Herbomel, P. (2006). Tracing hematopoietic precursor migration to successive hematopoietic organs during zebrafish development. Immunity *25*, 963–975.

Nguyen-Chi, M., Laplace-Builhe, B., Travnickova, J., Luz-Crawford, P., Tejedor, G., Phan, Q.T., Duroux-Richard, I., Levraud, J.P., Kissa, K., Lutfalla, G., et al. (2015). Identification of polarized macrophage subsets in zebrafish. Elife *4*, e07288.

van Niel, G., D'Angelo, G., and Raposo, G. (2018). Shedding light on the cell biology of extracellular vesicles. Nat. Rev. Mol. Cell Biol. *19*, 213–228.

Okabayashi, S., and Kimura, N. (2010). LGI3 interacts with flotillin-1 to mediate APP trafficking and exosome formation. NeuroReport *21*, 606–610.

Oliveros, J.C. (2007). VENNY. An Interactive Tool for Comparing Lists with Venn Diagrams. BioinfoGP of CNB-CSIC, http://bioinfogp.cnb.csic.es/tools/venny/.

Ostrowski, M., Carmo, N.B., Krumeich, S., Fanget, I., Raposo, G., Savina, A., Moita, C.F., Schauer, K., Hume, A.N., Freitas, R.P., et al. (2010). Rab27a and Rab27b control different steps of the exosome secretion pathway. Nat. Cell Biol. *12*, 19–30.

Paggetti, J., Haderk, F., Seiffert, M., Janji, B., Distler, U., Ammerlaan, W., Kim, Y.J., Adam, J., Lichter, P., Solary, E., et al. (2015). Exosomes released by chronic lymphocytic leukemia cells induce the transition of stromal cells into cancer-associated fibroblasts. Blood *126*, 1106–1117.

Peinado, H., Alečković, M., Lavotshkin, S., Matei, I., Costa-Silva, B., Moreno-Bueno, G., Hergueta-Redondo, M., Williams, C., García-Santos, G., Ghajar, C.M., et al. (2012). Melanoma exosomes educate bone marrow progenitor cells toward a pro-metastatic phenotype through MET. Nat. Med. *18*, 883–891.

Peinado, H., Zhang, H., Matei, I.R., Costa-Silva, B., Hoshino, A., Rodrigues, G., Psaila, B., Kaplan, R.N., Bromberg, J.F., Kang, Y., et al. (2017). Pre-metastatic niches: organ-specific homes for metastases. Nat. Rev. Cancer *17*, 302–317.

Plebanek, M.P., Angeloni, N.L., Vinokour, E., Li, J., Henkin, A., Martinez-Marin, D., Filleur, S., Bhowmick, R., Henkin, J., Miller, S.D., et al. (2017). Pre-metastatic cancer exosomes induce immune surveillance by patrolling monocytes at the metastatic niche. Nat. Commun. *8*, 1319.

Pucci, F., Garris, C., Lai, C.P., Newton, A., Pfirschke, C., Engblom, C., Alvarez, D., Sprachman, M., Evavold, C., Magnuson, A., et al. (2016). SCS macrophages suppress melanoma by restricting tumor-derived vesicle-B cell interactions. Science *1328*, 242–246.

Raposo, G., and Stoorvogel, W. (2013). Extracellular vesicles: exosomes, microvesicles, and friends. J. Cell Biol. *200*, 373–383.

Roh-Johnson, M., Shah, A.N., Stonick, J.A., Poudel, K.R., Kargl, J., Yang, G.H., di Martino, J., Hernandez, R.E., Gast, C.E., Zarour, L.R., et al. (2017). Macrophage-dependent cytoplasmic transfer during melanoma invasion in vivo. Dev. Cell *43*, 549–562.e6.

Saunderson, S.C., Dunn, A.C., Crocker, P.R., and McLellan, A.D. (2014). CD169 mediates the capture of exosomes in spleen and lymph node. Blood *123*, 208–216.

Schindelin, J., Arganda-Carreras, I., Frise, E., Kaynig, V., Longair, M., Pietzsch, T., Preibisch, S., Rueden, C., Saalfeld, S., Schmid, B., et al. (2012). Fiji: an open-source platform for biological-image analysis. Nat. Methods *9*, 676–682.

Spilsbury, K., O'Mara, M.A., Wu, W.M., Rowe, P.B., Symonds, G., and Takayama, Y. (1995). Isolation of a novel macrophage-specific gene by differential cDNA analysis. Blood *85*, 1620–1629.

Stoletov, K., Kato, H., Zardouzian, E., Kelber, J., Yang, J., Shattil, S., and Klemke, R. (2010). Visualizing extravasation dynamics of metastatic tumor cells. J. Cell Sci. *123*, 2332–2341.

Takahashi, Y., Nishikawa, M., Shinotsuka, H., Matsui, Y., Ohara, S., Imai, T., and Takakura, Y. (2013). Visualization and in vivo tracking of the exosomes of murine melanoma B16-BL6 cells in mice after intravenous injection. J. Biotechnol. *165*, 77–84.

Takov, K., Yellon, D.M., and Davidson, S.M. (2017). Confounding factors in vesicle uptake studies using fluorescent lipophilic membrane dyes. J. Extracell. Vesicles *6*, 1388731.

Taylor, M.J., Perrais, D., and Merrifield, C.J. (2011). A high precision survey of the molecular dynamics of mammalian clathrin-mediated endocytosis. PLoS Biol. *9*, e1000604.

Théry, C., Amigorena, S., Raposo, G., and Clayton, A. (2006). Isolation and characterization of exosomes from cell culture supernatants. Curr. Protoc. Cell Biol. 3.22.1–3.22.29.

Thomas, P.D., Campbell, M.J., Kejariwal, A., Mi, H., Karlak, B., Daverman, R., Diemer, K., Muruganujan, A., and Narechania, A. (2003). PANTHER: A library of protein families and subfamilies indexed by function. Genome Res. *13*, 2129–2141.

Verweij, F., Revenu, C., Arras, G., Dingli, F., Loew, D., Pegtel, M., Follain, G., Allio, G., Goetz, J.G., Zimmermann, P., et al. (2019). Live tracking of inter-organ communication by endogenous exosomes in vivo. Dev. Cell *48*, this issue, 573–589.

Vogel, D.Y.S., Heijnen, P.D.A.M., Breur, M., de Vries, H.E., Tool, A.T.J., Amor, S., and Dijkstra, C.D. (2014). Macrophages migrate in an activation-dependent manner to chemokines involved in neuroinflammation. J. Neuroinflamm. *11*, 1–11.

Van Der Vos, K.E., Abels, E.R., Zhang, X., Lai, C., Carrizosa, E., Oakley, D., Prabhakar, S., Mardini, O., Crommentuijn, M.H.W., Skog, J., et al. (2016). Directly visualized glioblastoma-derived extracellular vesicles transfer RNA to microglia/macrophages in the brain. Neuro. Oncol. *18*, 58–69.

White, R., Rose, K., and Zon, L. (2013). Zebrafish cancer: the state of the art and the path forward. Nat. Rev. Cancer *13*, 624–636.

Whiteside, T.L. (2016). Exosomes and tumor-mediated immune suppression. J. Clin. Invest. *126*, 1216–1223.

Würthner, F., Kaiser, T.E., and Saha-Möller, C.R. (2011). J-aggregates: From serendipitous discovery to supramolecular engineering of functional dye materials. Angew. Chem. Int. Ed. *50*, 3376–3410.

Xiao, M., Zhang, J., and Chen, W., Chen W. (2018). M1-like tumor-associated macrophages activated by exosome-transferred THBS1 promote malignant migration in oral squamous cell carcinoma. J. Exp. Clin. Cancer Res. *37*, 1–15.

Zomer, A., Maynard, C., Verweij, F.J., Kamermans, A., Schäfer, R., Beerling, E., Schiffelers, R.M., De Wit, E., Berenguer, J., Ellenbroek, S.I.J., et al. (2015). In vivo imaging reveals extracellular vesicle-mediated phenocopying of metastatic behavior. Cell *161*, 1046–1057.

STAR★METHODS

KEY RESOURCES TABLE

REAGENT OR RESOURCE	SOURCE	IDENTIFIER
Chemicals, Peptides and Recombinant proteins		
MemBright	Collot et al. (2019)	N/A
PKH-26	Sigma-Aldrich	MINI26
100nm fluorescent beads	Phosphorex	2211
Antibodies		
Mouse monoclonal anti-Alix antibody	BD Biosciences	Cat# 611621; RRID: AB_2236941
Mouse monoclonal anti-TSG-101 antibody	GeneTex	Cat# GTX70255; RRID: AB373239
Anti-mouse IgG coupled to HRP	Fisher scientific	Cat# NC9491974
Deposited Data		
EV related experimental details	EV-track consortium	EV180078
EV proteomics	Exocarta	TBD
Experimental Models: Cell lines		
Zmel1	White lab (MSKCC)	N/A
Zmel1 tdTomato	White lab (MSKCC)	N/A
Zmel1 Syntenin2-GFP	This paper	N/A
AB9	ATCC	ATCC-CRL-2298
4T1		RRID: CVCL_0125
4T1 CD63-GFP	This paper	N/A
B16F0	ATCC	ATCC CRL-6322; RRID: CVCL_0604
B16F1	ATCC	ATCC CRL-6323; RRID: CVCL_0158
B16F10	ATCC	ATCC CRL-6475; RRID: CVCL_0159
451-LU	Soengas lab (CNIO)	RRID: CVCL_6357
SK-Mel28	Soengas lab (CNIO)	RRID: CVCL_0526
SK-Mel147	Soengas lab (CNIO)	RRID: CVCL_3876
SK-Mel103	Soengas lab (CNIO)	RRID: CVCL_6069
WM35	Soengas lab (CNIO)	RRID: CVCL_0580
WM164	Soengas lab (CNIO)	RRID: CVCL_7928
Experimental Models: Organisms/strains		
Zebrafish: *Tg(Fli1a:eGFP)*	Peri lab; EMBL zebrafish facility	N/A
Zebrafish: *Tg(mpeg1a:eGFP)*	Lengerke lab; Basel University zebrafish facility	N/A
Zebrafish: *Tg(mpo:eGFP)*	Lengerke lab; Basel University zebrafish facility	N/A
Zebrafish: *Tg(Fli1a:Gal4; UAS:RFP)*	Lengerke lab; Basel University zebrafish facility	N/A
Zebrafish: Casper *Tg(Flk:eGFP; Gata1:RFP)*	Vermot lab; IGBMC zebrafish facility	N/A
Zebrafish: *Tg(mpeg1:mCherry; TNFa:eGFP)*	Djouad lab; IRMB zebrafish facility	N/A
Recombinant DNA		
pSyntenin2-eGFP	Zimmermann lab (CRCM)	N/A
pCS2 Zf-Syntenin2-eGFP	This paper	N/A
pLenti CMV-CD63-AcGFP	This paper	N/A
Software and Algorithms		
Fiji / Image J	NIH	N/A
IMOD	University of Colorado	N/A
Amira for Life Sciences	ThermoFisher Scientific	N/A
GraphPad PRISM	GraphPad Software	N/A
MaxQuant	Max Planck Institute of Biochemistry	N/A
PyCorrFit software	Max Planck Institute of Biochemistry	N/A

(*Continued on next page*)

Continued

REAGENT OR RESOURCE	SOURCE	IDENTIFIER
Other		
Transmitted electron microscope CM12	Philips	N/A
Transmitted electron microscope CM120	Philips	N/A
Biotwin CM120 (FEI) TEM	Philips	
Nanosight NS300	Malvern Instruments	N/A
ZetaView	Particle Metrix	N/A
NanoAcquity UPLC device	Waters	N/A
NanoLC-Ultra 1D+ system	Eksigent	N/A
Cary 400 Scan ultraviolet–visible spectrophotometer	Varian	N/A
FluoroMax-4 spectrofluorometer	Horiba Jobin Yvon	N/A
M205 FA stereomicroscope	Leica	N/A
Inverted TCS SP5 confocal microscope	Leica	N/A
Upright SP8 confocal microscope	Leica	N/A

CONTACT FOR REAGENT AND RESOURCE SHARING

Further information and requests for resources and reagents should be directed to and will be fulfilled by the Lead Contact, Vincent Hyenne (hyenne@unistra.fr).

EXPERIMENTAL MODEL AND SUBJECT DETAILS

Zmel1, Zmel1 tdTomato and Zmel1 Syntenin2-GFP

Zebrafish melanoma Zmel1 and Zmel1 td Tomato Kindly provided by Richard White (Memorial Sloan Kettering Cancer Center, New York) (Heilmann et al., 2015). Zmel1 Syntenin2-GFP generated in the laboratory. Culture condition: 28°C, 5% CO_2. DMEM high glucose (HG), 10% FBS, 1% NEAA-MEM, 1% penicillin-streptomycin.

AB9 Cells

Zebrafish fibroblasts obtained from the caudal fin of an adult AB strain zebrafish (ATCC CRL-2298). Culture condition: 28°C, 5% CO_2. DMEM HG, 10% FBS, 1% NEAA-MEM, 1% Penstrep.

4T1 Cells and 4T1 CD63-GFP

Mouse mammary gland carcinoma (BALB/c female) (CVCL_0125). 4T1 CD63-GFP generated in the laboratory. Culture condition: 37°C, 5%CO_2. RPMI 1640 with 10% FBS, 1% penicillin-streptomycin. Authentication: Injection in the nipple of mammary gland of BALB/c mice lead to mammary tumor.

B16-F0, F1 and F10

Mouse melanoma cell lines, purchased from ATCC (ATCC CRL-6322; ATCC CRL-6323; ATCC CRL-6475). Culture condition: 37°C, 5%CO_2. DMEM supplemented with 10% (v/v) EV-depleted fetal bovine serum (EV-d-FBS), glutamine 2mM and gentamicin

451-LU, SK-Mel28, SK-Mel147, SK-Mel103, WM35 and WM164

Human melanoma cells, kindly provided by Dr. M. Soengas (CNIO, Madrid). Culture condition: 37°C, 5%CO_2. DMEM with 10% EV-d-FBS.

Zebrafish

Zebrafish embryos were obtained from the following strains: *Tg(fli1a:eGFP), Tg(mpeg1:eGFP)*, *Tg(mpo:eGFP), Tg(Fli1:Gal4; UAS: RFP), Casper Tg(Gata1:RFP; flk:GFP), Tg(mpeg:mCherry*; TNF-α:GFP). Embryos were grown in our laboratory or kindly provided by F. Peri's (EMBL, Heidelberg, Germany) and C. Lengerke's laboratories (University Hospital Basel, Switzerland). Embryos were maintained at 28° in Danieau 0.3X medium, supplemented with 1-Phenyl-2-thiourea (Sigma-Aldrich) after 24 h post fertilization (hpf). For all Zebrafish experiments, the offspring of one single cross was selected, based on anatomical/developmental good health. Embryos were split randomly between experimental groups. All injection experiments were carried at 48 hpf and imaged between 48 hpf and 72 hpf. All animal procedures were performed in accordance with French and European Union animal welfare guidelines and supervised by local ethics committee (Animal facility #A6748233; APAFIS #2018092515234191).

METHOD DETAILS

Cell Line Generation

To generate Zmel1 cells expressing Syntenin2-GFP, Syntenin2 (a gift from P.Zimmerman) was first cloned in pCS2 eGFP Ires Blast vector. Then, 2 millions of Zmel dark cells were transfected with 2 μg of plasmid pCS2 Zf-Syntenin2-eGFP Ires Blast cut with NotI using 4 μl of JetPrime according to manufactory instructions (PolyPlus, Illkirch, France). After 1 week, cells with stable integration of the construct were selected using 4μg/ml of blasticidin (Sigma Aldrich, St. Quentin Fallavier, France). 4T1 cells expressing CD63-GFP were generated as follows. Briefly, human CD63 cDNA was fused to AcGFP cDNA by In-Fusion cloning (Takara, Ozyme, Saint-Quentin-en-Yvelines, France) and introduced in pLenti CMV-MABBXXS mPGK-Blast vector. Lentiviruses were obtained by HEK293T cells (ATCC CRL-3216; cultured in DMEM, 10% FCS, 1% penicillin-streptomycin) transfection (Invitrogen, Life Technologies, Saint Aubin, France) with pLenti CMV-CD63-acGFP mPGK-Blast together with pLP1, pLP2 and pLP/VSVG lentiviral packaging plasmids to obtain lentiviral particles. After 48 hours, conditioned media was collected, filtered through a 0.22 μm filter to remove cell debris, and used to transduce 4T1 cells cultured in DMEM supplemented with 10% fetal calf serum and 1% penicillin-streptomycin (Gibco, USA) in the presence of 5μg/mL polybrene (Sigma Aldrich, Lyon, France), followed by selection with puromycin (1 μg/mL, Sigma Aldrich, Lyon, France). Human blood was collected from healthy donors using 3.8% (v/v) sodium citrate (1:9) as anticoagulant. Human erythrocyte rich pellet was obtained by centrifugation at 250 rpm during 15 minutes at room temperature.

EV Isolation and Analysis

For Zmel1 and 4T1 EVs isolation, cells were cultured in EV depleted medium (obtained by overnight ultracentrifugation at 100,000g, using a Beckman, XL-70 centrifuge with a Ti70 rotor) for 24h before supernatant collection. Extracellular medium was concentrated using a Centricon Plus-70 centrifugal filter (10k; Millipore) and EVs were isolated by successive centrifugation at 4°C: 5 minutes at 300 g, 10 minutes at 2,000 g, 30 minutes at 10,000 g and 70 minutes at 100,000 g (using a Beckman XL-70 centrifuge with a SW28 rotor). EVs pellets were washed in PBS, centrifuged again at 100,000 g for 70 minutes, resuspended in PBS and stored at 4°C. For *in vivo* experiments, EVs were used immediately after isolation or kept 4°C at and used the next day.

For mouse and human melanoma EVs isolation, cells were cultured in media supplemented with 10% EV-depleted FBS (FBS, Hyclone). FBS was depleted of bovine EVs by ultracentrifugation at 100,000xg for 70 min. EVs were isolated from conditioned media collected after 72 h of cell cultures by successive centrifugation at 10°C: 5 minutes at 300 g, 10 minutes at 500 g, 20 minutes at 12,000 g and 70 minutes at 100,000 g (using a Beckman Optima X100 with a Beckman 70Ti rotor). EVs pellets were washed in PBS, centrifuged again at 100,000 g for 70 minutes, and resuspended in PBS. Protein content was measured by bicinchoninic acid assay (BCA assay).

For transmitted electron microscopy analysis, 3 μl of EV extracts were allowed to dry on formvar coated grids for 20 minutes, fixed in 3% PFA for 10 minutes, rinsed in water and contrasted in a uranyl acetate (0,4%)/ methylcellulose (2%) mix for 10 minutes on ice. EVs were observed either with an Orius 100 charge-coupled device camera (Gatan) mounted on a Philips CM12 microscope operated at 80kV or with a Veleta 2kx2k side-mounted TEM CDD Camera (Olympus Soft Imaging Solutions) mounted on a Philips CM120 microscope operated at 120kV.

NTA was performed on Zmel1 EVs diluted 10 times with sterile PBS, using a Nanosight NS300 (Malvern Instruments) or a ZetaView (Particle Metrix). The measurement was repeated three times.

For density gradient analysis, EVs isolated in the 100,000 g pellet were loaded on top of a 5-40% iodixanol (Optiprep) density gradient prepared as previously described (Van Deun et al., 2014). The gradient was centrifuged for 18 hours at 100,000g and 4°C (using a Beckman XL-70 centrifuge with a SW28 rotor). Gradient fractions of 1ml were collected from the top of the gradient. Fractions 1 to 4, 5 to 10 and 11 to 16 were pooled, diluted to 16 ml in PBS and centrifuged for 3 hours at 100,000g and 4°C. The resulting pellet was resuspended in 50 μl of PBS. For western blotting analysis, 10 μl of EV extracts were loaded on 4-20% polyacrylamide gels (Biorad), under denaturing conditions. The following antibodies were used: Alix (BD Biosciences 611621) and TSG101 (GeneTex GTX70255). Acquisitions were done using a PXi system (Syngene).

Shotgun Proteomics

Sample Preparation of Zmel1 EVs Protein Content

After having determined protein concentration (RC-DC™; Bio-Rad, Hercules, CA), 20 μg samples were denaturated at 95°C for 5 min in Laemmli buffer and then concentrated in one stacking band using a 5% SDS-PAGE gel. The gel was fixed with 50% ethanol/3% phosphoric acid and stained with colloidal Coomassie Brilliant Blue. Each band was excised, cut in five pieces, and transferred into a 96-well microtiter plate. Gel slices were washed with 3 cycles of incubations in 100 μL of 50:50 (v/v) 25 mM NH_4HCO_3/ACN for 10 min. Gel bands were then dehydrated with 50 μL 100% ACN and then reduced with 50 μL 10 mM DTT for 30 min at 60°C, followed by 30 min at RT. Proteins were then alkylated with 50 μL 55 mM iodoacetamide for 20 min in the dark at RT, and then 100 μL ACN were added for 5 min. Samples were washed with 50 μL 25 mM NH_4HCO_3 for 10 min, and then 50 μL ACN for 5 min, before being dehydrated with two cycles of incubations in 50 μL ACN for 5 min. Proteins were digested overnight with a modified porcine trypsin (Promega, Madison, WI) solution at a 1:100 (w/w) enzyme/protein ratio at 37°C. Tryptic peptides were extracted under agitation at RT with 60 μL 60% ACN/0.1% FA for 45 min, and then 100% ACN for 10 min. The extraction supernatants were pooled and vacuum-dried, before re-suspension in 40 μL 2% ACN/0.1% FA.

Nano-LC-MS/MS Analysis of Zmel1 EVs Protein Content

Nano-LC-MS/MS analysis was performed on a nanoAcquity UPLC device (Waters, Milford, MA) coupled to a Q-Exactive Plus mass spectrometer (Thermo Fisher Scientific, Bremen, Germany). The solvents consisted of 0.1% FA in H_2O (solvent A) and 0.1% in ACN (solvent B). 1 μL of the samples was loaded onto a Symmetry C18 pre-column (20 mm × 180 μm, 5 μm diameter particles; Waters, Milford, MA) over 3 min at 5 μL/min with 1% solvent B. Peptides were eluted on a Acquity UPLC BEH130 C18 column (250 mm × 75 μm, 1.7 μm particles; Waters, Milford, MA) at 450 μL/min with the following gradient of solvent B: linear from 1% to 8 % in 2 min, linear from 8% to 35% in 77 min, linear from 35% to 90% in 1 min, isocratic at 90% for 5 min, down to 1% in 2 min, isocratic at 1% for 2 min.

The Q-Exactive Plus was operated in data-dependent acquisition mode by automatically switching between full MS and consecutive MS/MS acquisitions. Full-scan MS spectra were collected from 300-1,800 m/z at a resolution of 70,000 at 200 m/z with an automatic gain control target fixed at 3×10^6 ions and a maximum injection time of 50 ms. The top 10 precursor ions with an intensity exceeding 2×10^5 ions and charge states ≥ 2 were selected on each MS spectrum for fragmentation by higher-energy collisional dissociation. MS/MS spectra were collected at a resolution of 17,500 at 200 m/z with a fixed first mass at 100 m/z, an automatic gain control target fixed at 1×10^5 ions and a maximum injection time of 100 ms. A dynamic exclusion time was set to 60 s.

Sample Preparation of Mammalian EVs Cargo

Proteins were solubilized using 8 M urea in 100 mM Tris-HCl pH 8.0. Samples (7.5 μg) were digested by means of the standard FASP protocol. Briefly, proteins were reduced (10 mM DTT, 30 min, RT), alkylated (55 mM IA, 20 min in the dark, RT) and sequentially digested with Lys-C (Wako) (protein:enzyme ratio 1:50, o/n at RT) and trypsin (Promega) (protein:enzyme ratio 1:100, 6 h at 37° C). Resulting peptides were desalted using C_{18} stage-tips.

Nano-LC-MS/MS Analysis of Mammalian EVs Cargo

LC-MS/MS was done by coupling a nanoLC-Ultra 1D+ system (Eksigent) to a LTQ Orbitrap Velos mass spectrometer (Thermo Fisher Scientific) via a Nanospray Flex source (Thermo Fisher Scientific). Peptides were loaded into a trap column (NS-MP-10 BioSphere C18 5 μm, 20 mm length, Nanoseparations) for 10 min at a flow rate of 2.5 μl/min in 0.1% FA. Then peptides were transferred to an analytical column (ReproSil Pur C18-AQ 2.4 μm, 500 mm length and 0.075 mm ID) and separated using a 120 min linear gradient (buffer A: 4% ACN, 0.1% FA; buffer B: 100% ACN, 0.1% FA) at a flow rate of 250 nL/min. The gradient used was: 0-2 min 6% B, 2-103 min 30% B, 103-113 min 98% B, 113-120 min 2% B. The peptides were electrosprayed (1.8 kV) into the mass spectrometer with a PicoTip emitter (360/20 Tube OD/ID μm, tip ID 10 μm) (New Objective), a heated capillary temperature of 325°C and S-Lens RF level of 60%. The mass spectrometer was operated in a data-dependent mode, with an automatic switch between MS and MS/MS scans using a top 15 method (threshold signal $\geq$ 800 counts and dynamic exclusion of 60 s). MS spectra (350-1500 m/z) were acquired in the Orbitrap with a resolution of 60,000 FWHM (400 m/z). Peptides were isolated using a 1.5 Th window and fragmented using collision induced dissociation (CID) with linear ion trap read out at a NCE of 35% (0.25 Q-value and 10 ms activation time). The ion target values were 1E6 for MS (500 ms max injection time) and 5000 for MS/MS (100 ms max injection time).

Nano-LC-MS/MS Data Interpretation

Raw files were processed with MaxQuant (versions 1.6.0.16) (Cox et al., 2014) against an in-house concatenated *Danio rerio-Bos taurus* (UniProtKB, February 2017, 90,922 entries) supplemented with contaminants for Zmel1 EVs proteins and generated with the database toolbox from MSDA (Carapito et al., 2014), or a human protein database (UniProtKB/Swiss-Prot, August 2014, 20,187 sequences) supplemented with contaminants for mammalian EVs cargo. Label-free quantification was done with the match between runs option activated (match window of 0.7 min and alignment window of 20 min). Carbamidomethylation of cysteines was set as a fixed modification whereas oxidation of methionines and protein N-term acetylation were set as variable modifications. Minimal peptide length was set to 7 amino acids and a maximum of two tryptic missed-cleavages were allowed.

Protein Comparisons

To compare the Zmel1 protein content with mammalian EV content, each protein list was concatenated and duplicate proteins were deleted. Ortholog proteins were searched using the ortholog protein files predicted by the PANTHER classification system (ftp://ftp.pantherdb.org/ortholog/13.0/ (Thomas et al., 2003)). Only proteins referred as ''Least diverged ortholog'' or ''Ortholog'' were considered. All comparisons between Zmel1 EVs and mammalian EVs were done using human orthologs and the lists of common proteins was obtained using Venny 2.1 (Oliveros, 2007).

MemBright and PKH Labeling of EVs

Isolated EVs were incubated with MemBright-Cy3 or Cy5 at 200nM (final concentration) in PBS for 30 minutes at room temperature in the dark. They were then rinsed in 15ml of PBS and centrifuged at 100,000g with a SW28 rotor in a Beckman XL-70 centrifuge. Pellets were resuspended in 50 μl PBS and stored at 4°C. For *in vivo* experiments, EVs were used immediately after isolation or stored overnight at 4°C and injected the next day. For PKH-26 labeling EVs were treated according to the manufacturer's instructions (2 μM final concentration). Briefly, EVs in 200 μl of PBS were first mixed with 300 μl of Diluent C, then with 500μl of Diluent C containing 4 μl of PKH and finally incubated for 30 minutes at room temperature in the dark. PKH labeled EVs were then processed as MemBright labeled EVs. As a control, PBS alone was processed similarly to EVs, labeled with MemBright or PKH and analysed by microscopy or spectroscopy.

For photonic microscopy analysis, 3 μl of labeled EV extracts were allowed to settle on poly-L lysine coated coverslips and then imaged on a Zeiss Imager Z2 with a 63X objective (N.A. 1.4) or with a SP5 confocal (Leica) with a 40X objective (N.A. 1.25).

Spectroscopy

EVs labeled with either MemBright-Cy3 or PKH-26, or control MemBright-Cy3 or control PKH (diluted in PBS as described above), as well as the dyes directly diluted in Milli-Q water (Millipore) or ethanol were analyzed by spectroscopy. Absorption and emission spectra were recorded at 20°C in quartz cuvettes on a Cary 400 Scan ultraviolet–visible spectrophotometer (Varian) and a FluoroMax-4 spectrofluorometer (Horiba Jobin Yvon) equipped with a thermostated cell compartment, respectively. For standard recording of fluorescence spectra, excitation was at 520 nm and the emission was collected 10 nm after the excitation wavelength (530 nm to 700 nm). All the spectra were corrected from wavelength-dependent response of the detector. The scattering due to the EVs was corrected with a baseline correction using Origin software. Quantum yields were determined using rhodamine B in water (QY= 0.31) as a reference (Magde et al., 1999).

Fluorescence Correlation Spectroscopy (FCS)

To characterize the size of PKH aggregates, FCS measurements were performed on PKH26 (diluted at 5 μM) using a home-built confocal set-up based on a Nikon inverted microscope with a Nikon 60x 1.2NA water immersion objective. Excitation was provided by a cw laser diode (532 nm, Oxxius) and photons were detected with a fibered Avalanche Photodiode (APD SPCM-AQR-14-FC, Perkin Elmer) connected to an on-line hardware correlator (ALV7000-USB, ALV GmbH, Germany). Typical acquisition time was 5 min (10 × 30 s) with an excitation power of 1.1 μW at the sample level. The data were analyzed using the PyCorrFit software (Müller et al., 2014).

MemBright Labeling of Cells

Sub-confluent cells in 10cm culture dishes were rinsed twice with warm serum free medium and then incubated for 30 minutes at 28°C (Zmel1 cells) or at 37°C (4T1 cells) with MemBright quickly diluted in serum free medium (200nM final). To eliminate all possible traces of unbound MemBright, cells were then rinsed three times with serum free medium, rinsed with EDTA and trypsinated. Cells were then either injected in zebrafish embryos, seeded in a triple flask for EV production, or seeded in glass bottom microwell dishes (MatTek Corporation) pre-coated with fibronectin from bovine plasma at 10μg/ml (Sigma F-1141) for imaging.

Intravascular Injection of Zebrafish Embryo

At 48h post-fertilization (hpf), zebrafish embryos were dechorionated and mounted in 0.8% low melting point agarose pad containing 650 μM of tricaine (ethyl-3-aminobenzoate-methanesulfonate) to immobilize them. Pre-labelled EVs, polystyrene beads (Phosphorex) or tumors cells were injected with a Nanoject microinjector 2 (Drummond) and microforged glass capillaries (25 to 30 μm inner diameter) filled with mineral oil (Sigma). 27,6 nL of a EV, beads or cell suspension (at 100.10^6 cells) per ml were injected into the duct of Cuvier of the embryos under the M205 FA stereomicroscope (Leica), as previously described (Follain et al., 2018b; Stoletov et al., 2010). For the priming experiments, 32hpf embryos were injected with either Zmel1 EVs or 100nm polystyrene beads (together with fluorescent dextran to assess the efficiency of injection). 14h post-injection, embryos were injected in the circulation with Zmel1 tdTomato tumor cells. Larvae were grown for a week and imaged at 7 days post-injection. For late endosome/lysosome labeling, embryos were incubated with Lysotracker Deep Red (Thermo Fisher Scientific) diluted at 5μM in Danieau 0,3X medium for 2 hours at 28°C before injection.

Confocal Imaging and Analysis

Confocal imaging was alternatively performed with an inverted TCS SP5 with HC PL APO 20X/0,7 IMM CORR CS objective (Leica) or an upright SP8 confocal microscope with a HC FLUOTAR L 25X/0,95 W VISIR objective (Leica). For high speed imaging of EVs in the blood flow, embryos were imaged right after injection; acquisitions were done at 80-100 frames per second for 1 minute, using the resonant scanner in a single Z plane, with an opened pinhole of more than 1 airy unit. To identify the cell types uptaking EVs, the caudal plexus region of mpeg1:GFP, mpo:GFP or Fli1a:GFP was imaged 3h post-injection with a z-step of 1 μm. To quantify the proportion of EVs arrested in the dorsal aorta *vs* venous plexus regions, images were acquired similarly in Fli1:GFP embryos. For each case, quantification is described in the next paragraphs. To image the dynamics of macrophage protrusions, short time lapses of mpeg1:GFP embryos were acquired at 5 to 10 Z stacks per minute (z-step of 0,5 μm, stack covering the macrophage). To image the dynamics of macrophages, long time lapses of mpeg1:GFP embryos were acquired at 1 Z stack per minute for one hour in (z-step of 2 μm, stack covering the venous plexus). To image the uptake of EVs by macrophage, mpeg1:GFP embryos short time lapses were generated right after injection at 3 to 8 images per second on single Z planes. Image analysis and processing were performed using Fiji (Schindelin et al., 2012) as described in the following paragraphs.

Semi-automated Method to Determine the Proportion of Internalized EVs

To determine the proportion of EVs internalized by either endothelial or macrophages, we used the Z-stacks obtained from either Fli1:GFP or mpeg1:GFP embryos injected with Zmel1-MemBright EVs. Using Fiji, we split the cell and EVs channels and merged them in a single RGB image. From the merged channel, we made a binary stack followed by a Z-projection with maximal intensity. We used this as a reference image where all the EVs and cells are apparent. After normalizing this image to 1 we multiplied each stack (respectively EVs and Cell) by this projection. In both stacks, we thus kept only the positions that colocalize either with the EV position or the Cells position (all other positions possess a null value). We then made a binary from the Cell stack, applied close and dilated before normalizing it to 1. The multiplication of this stack with the EV one lead to a new stack that keeps only the particle enclosed in

the cellular compartments. Getting back to the Cell stack, we apply an inversion of the intensity values before substracting 254. The resulting stack was then multiplied by the EV stack and the created new stack let only apparent the EVs that did not colocalize with the cells. Further analyses of the intensities from the two stacks allowed us to access the ratiometric values of EVs uptaken by the different cell lines.

Quantification of EVs in Aorta vs Vein Regions

Each region (dorsal aorta and venous plexus) was manually delimited on Z-projections, using vessels visible in Fli1:GFP channels. Total EV intensity was then measured in each region and reported to the area. A ratio of EV fluorescence in the venous plexus over dorsal aorta was then measured for each fish.

Flow Analysis for Red Blood Cells

Flow analysis of red blood cells

We first globally enhanced the contrast of the whole stack. Then we performed a Z-projection with the average intensity and subtracted the obtained image to the stack. The remaining stack exhibits only the moving objects i.e. the red blood cells in this case. Then we applied a binarisation to the stack before applying a bandpass filter with the correct values to remove the background noise and keeping only the flowing blood cells. This stack was then further analyzed with the Mosaic 2D/3D particle tracker plugin. We thus accessed the positions of each blood cell for the different frames and we computed the velocities of each individual track.

Flow Analysis of EVs

Time-lapses of EVs were first thresholded and binarized. We then inverted the stack before running the 2D spot enhancing Filter plugin. We used the resulting stack to perform a second binarisation and then launched the Mosaic 2D/3D particle tracker plugin. We thus accessed the positions of each EV for the different frames and we computed the velocities of each individual track

EVs and RBCs Distance and Velocity from the Endothelial Barrier

In order to access to the distance of the EVs or red blood cells to the endothelial barrier, we first drew the endothelial wall using the transmitted light and extracted its coordinates to a table. From the analysis described in the previous paragraph, we extracted the coordinates and the velocity EVs and red blood cells. We ran a macro where we compared for all the position X_{EV} and Y_{EV} of the EV the closest position X_{endo} and Y_{endo} by comparing all the possible distances d by calculating :

$$d = \sqrt{(x_{EV} - x_{endo})^2 + (y_{EV} - y_{endo})^2}$$

and keeping the smallest distance.

This allowed us to plot the EV or the red blood cells velocities as a function of the distance from the endothelial wall.

Sample Preparation for Correlative Light and Electronic Microscopy of ZF Embryos

Correlative Light and Electron Microscopy was performed as previously described (Goetz et al., 2014; Karreman et al., 2016a). Transgenic mpeg1:GFP embryos were injected with MemBright-Cy3 4T1 EVs and imaged alive with a Leica SP8 confocal microscope (see "Confocal imaging and analysis section"). Z stack was performed on two patrolling macrophages having uptaken EVs. After imaging, the embryo was chemically fixed with 2,5% glutaraldehyde and 4% paraformaldehyde in 0.1 M Cacodylate buffer (the fish tail was cut off in the fixative). The sample was kept in fixative at room temperature for 1-2h and stored in fixative at 4°C overnight or until further processing. The sample was rinsed in 0.1M Cacodylate buffer for 2x5min and post-fixed using 1% OsO4 in 0.1 M Cacodylate buffer, for 1h at 4°C. Then, sample was rinsed for 2x10 min in 0.1M Cacodlyate buffer and secondary post-fixed with 4% water solution of uranyl acetate, 1h at room temperature. Rotation was used at all steps of sample processing. Followed by 5 min wash in MiliQ water, the sample was stepwise dehydrated in Ethanol (25%, 50% each 15min, 95%, 3X100% each 20 min) and infiltrated in a graded series of Epon (Ethanol/Epon 3/1, 1/1, 1/3, each 45 min). Sample was left in absolute Epon (EmBed812) overnight. The following day, sample was placed in a fresh absolute Epon for 1h and polymerized (flat embedded) at 60°C for 24-48h. Once polymerized, most surrounding Epon was cut off using razorblade and sample was mounted on empty Epon blocks (samples flat on the top of the blocks) and left at 60°C for 24h-48h. Samples were attached to an imaging pin with dental wax and mounted into the Brukker Skyscan 1272 for microCT imaging. Data were acquired over 188° with 0.2° angular step and a pixel size of 9 μm. Karreman et al. thoroughly details the process of how the microCT data enables the correlation of fluorescent imaging to 3D EM of voluminous samples (Karreman et al., 2016a). Retrieval of the region of interest is described in Figure S4. The region of interest was targeted by ultramicrotome, sections stained with toluidine blue and compared with the MicroCT and LM datasets. After targeting, serial 70nm sections were collected in formvar coated slot grids. The sections were post stained with uranyl acetate (4%) and lead citrate. The sections were imaged in a Biotwin CM120 Philips (FEI) TEM at 80kV with a SIS 1K KeenView. Stitches of the 70 sections were aligned using the Track EM plugin in Fiji (Cardona et al., 2012). Segmentation and 3D reconstruction were done using the IMOD software package (Boulder Laboratory, University of Colorado) and Amira.

QUANTIFICATION AND STATISTICAL ANALYSIS

Statistical Tests

Statistical analysis of the results was performed using the GraphPad Prism program version 5.04. The Shapiro-Wilk normality test was used to confirm the normality of the data. The statistical difference of Gaussian data sets was analyzed using the Student unpaired two-tailed t test, with Welch's correction in case of unequal variances. For data not following a Gaussian distribution, the Mann-Whitney test was used. Illustrations of these statistical analyses are displayed as the mean +/- standard deviation (SD). p-values smaller than 0.05 were considered as significant. *, $p<0.05$, **, $p < 0.01$, ***, $p < 0.001$, ****, $p < 0.0001$.

Zebrafish Experiments

Measurements of EVs displacement in the dorsal aorta and in the caudal vein of zebrafish embryos (Figures 3B–3E) was performed on four zebrafish embryos. Measurements of EV uptake in aorta versus venous plexus was repeated three times (n=17; Figure 4B). Comparison of the uptake of beads, AB9 EVs and Zmel1 EVs by endothelial cells (n=20, 24 and 11 respectively; Figure 4C) and macrophages (n=28, 21 and 19 respectively; Figure 5C) was repeated three times each. The correlation between Zmel1 uptake intensity and macrophages perimeter was done on 73 macrophages (13 embryos; Figure 5B). The velocity of non-injected macrophages was measured on 35 macrophages (6 embryos; Figure 5E). The colocalization between uptaken EVs and lysotracker in macrophages at 10 min and 3h post-injection was performed on 61 and 54 puncta, respectively (n=6 and 7 fish, respectively; Figure 6D). The dynamics of macrophages injected with either beads or Zmel1 EVs was measured on 27 and 47 macrophages, respectively (5 and 8 embryos; Figure 8A). The activation of M1 macrophages after beads or Zmel1 EVs injection was repeated twice (n=38 and 28 fish, respectively; Figures 8B and 8C). The metastatic outgrowth of Zmel1 cells in zebrafish embryos injected with either beads or Zmel1 EVs was repeated five times (n=55 and 57 fish, respectively; Figure 8D).

EVs Experiments

Measurements of the diameters of Zmel1 EVs (Figure 1B) and Zmel1 EVs labeled with MemBright (Figure 2E) by NTA was repeated three times. Analysis of Zmel1 EVs (Figures 1C and 2D) and Zmel1 EVs labeled with MemBright (Figure 2D) by TEM was repeated each three times (n= 871 and 356, respectively). Spectroscopic analysis of PKH and MemBright labeled EVs (Figure 1B) was performed once, at different concentrations. Measurements of the fluorescence of PKH or MemBright labeled EVs was repeated three times (Figures S2A and S2B). The number of puncta measured is indicated in the graph bars. The density gradient isolation of EVs was repeated twice (Figure S1F). The measurements of the apparent EV diameter Vs beads diameter by confocal was repeated three times *in vitro* and *in vivo* (Figure S2). The number of individual puncta measured is indicated in the graphs. Mass spectrometry of EVs was performed on triplicates (Figure 1E; Table S1).

DATA AND SOFTWARE AVAILABILITY

The proteomics data have been deposited on Exocarta. All relevant data regarding the EVs experiments have been deposited on the EV-TRACK knowledgebase (EV-Track ID:EV180078) (Van Deun et al., 2017).